

The Photochemistry of Rydberg-Excited Cyclobutanone: Photoinduced Processes and Ground State Dynamics

J. Eng,¹ C. D. Rankine,² and T. J. Penfold¹

¹*Chemistry, School of Natural and Environmental Sciences, Newcastle University, Newcastle upon Tyne, NE1 7RU, UK*

²*Department of Chemistry, University of York, York, YO10 5DD, UK*

(*Electronic mail: tom.penfold@newcastle.ac.uk)

(*Electronic mail: julien.eng@newcastle.ac.uk)

(Dated: 15 February 2024)

Owing to ring-strain, cyclic ketones exhibit complex excited-state dynamics with multiple competing photochemical channels active on the ultrafast timescale. While the excited-state dynamics of cyclobutanone after $\pi^* \leftarrow n$ excitation into the lowest-energy excited singlet state (S_1) has been extensively studied, the dynamics following $3s \leftarrow n$ excitation into the higher-lying singlet Rydberg (S_2) state are less well understood. Herein, we couple quantum and excited-state trajectory surface-hopping molecular dynamics simulations to study the relaxation of cyclobutanone following $3s \leftarrow n$ excitation and to predict the ultrafast electron diffraction scattering signal that we anticipate to arise from the relaxation dynamics that we observe. Our simulations indicate that relaxation from the initially-populated singlet Rydberg state occurs on the hundreds-of-femtosecond to picosecond timescale consistent with the symmetry-forbidden nature of the state-to-state transition involved. Once cyclobutanone has relaxed non-radiatively to the electronic ground state (S_0), the vibrationally hot molecules have sufficient energy to form multiple fragmentary products on the electronic ground-state surface including $C_2H_4 + CH_2CO$ (**C2**; 20%), and $C_3H_6 + CO$ (**C3**; 2.5%). We discuss the limitations of our simulations, how these may influence the outcome of the excited-state dynamics we observe, and – ultimately – the predictive power of the simulated experimental observable.

I. INTRODUCTION

Ketones, *i.e.* organic compounds containing a carbonyl group, are among the simplest chromophores owing to their small size and low density of valence excited states. Consequently, their photochemistry has been intensively studied for several decades.^{1,2} Cyclic ketones form an important sub-class of these systems; despite their apparently equivalent simplicity, their photochemistry is often comparatively complex and features activity across multiple competing photochemical channels most commonly characterised by Norrish Type I processes. Here, upon excitation of an electron from the non-bonding orbital (n) on the carbonyl oxygen atom to the antibonding (π^*) molecular orbital of the carbonyl group, a carbon-carbon bond adjacent to the carbonyl (*i.e.* the carbon-carbon bond to the α carbon, Figure 1) cleaves, opening up the possibility of the formation of a variety of fragmentary products on the electronic ground-state surface after non-radiative relaxation. Amongst cyclic ketones, cyclobutanone has particular photochemistry owing to the high degree of ring strain in the cyclobutane ring (arising as a consequence of the small ring size).³ The particular photochemistry of cyclobutanone has attracted significant interest from both an experimental^{3–16} and theoretical^{17–24} perspective.

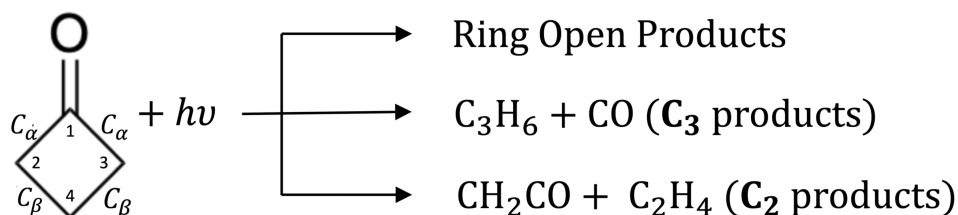


FIG. 1. Schematic of cyclobutanone and the potential photoproducts identified in previous work.

Many of these previous studies have aimed at elucidating the photochemistry and, in particular, the excited-state dynamics arising from excitation at the weak $S_1 \leftarrow S_0$ absorption band (*ca.* 330–240nm) associated with the symmetry-forbidden $\pi^* \leftarrow n$ transition. Early ultrafast spectroscopy carried out by Diau *et al.*¹⁰ reported that, upon excitation at 307 nm (*i.e.* slightly above energy of the $\pi^* \leftarrow n$ transition by *ca.* 2 kcal.mol^{−1}) α -cleavage occurs over a timescale of *ca.* 5 ps, driven initially by the C=O out-of-plane wagging, cyclobutane ring puckering, and C=O stretching modes. Following α -cleavage, a channel along which an S_1/S_0 conical intersection (CI) is encountered and *via* which non-radiative relaxation to the electronic ground state can proceed, cyclobutanone can undergo substantial structural changes that lead to the production of either i) a

vibrationally-hot S_0 species, ii) a diradical intermediate that fragments to yield $C_2H_4 + CH_2CO$ (**C2** products), or iii) the formation of $C_3H_6 + CO$ (**C3** products). The proposed fragmentation mechanism is consistent with the observed wavelength dependence of the **C3:C2** product ratios;^{4,7,8,13,25} this ratio is reported to be 0.5 on excitation at 313 nm, and increases to 0.8 at 248 nm and 1.0 at 200 nm.^{13,26} At wavelengths longer than 315 nm, there is a marked increase in the **C3:C2** product ratio; it is reported to be 2.0 at 326 nm and as high as 7.0 at 344 nm.^{7,26} The increase is indicative of an alternative mechanism in the S_1 state which becomes operational at longer wavelengths and it is proposed to involve photochemistry on the triplet manifold²⁶ as there is insufficient energy available to overcome the barrier encountered along the α -cleavage channel and reach the S_1/S_0 CI. This mechanistic picture is largely maintained in solution as demonstrated by Kao *et al.*³ who observed Norrish Type I α -cleavage on the sub-picosecond timescale, a consequence of excess vibrational energy available from UV-photon absorption from the electronic ground state. Kao *et al.*³ proposed that the observed wavelength dependence arose from the need to overcome a barrier on the S_1 surface (*e.g.* the barrier encountered along the α -cleavage channel). In addition, while triplet states have been invoked in the Norrish mechanism,¹³ Kao *et al.*³ reported that, even with sufficient excess vibrational energy available, triplet states may still play a mechanistic role although only in indirect channels active on timescales longer than 500 ps.

The second absorption band of cyclobutanone occurs between 206 to 182 nm and has been assigned to the $3s \leftarrow n$ transition into the second electronically-excited singlet state (S_2); a state that exhibits Rydberg character.¹⁴ Trentelman *et al.*¹⁵ have studied the 193 nm photolysis of cyclobutanone and have reported that 57% of the electronically-excited-state species form the **C3** products, 30% form the **C2** products in the electronically excited state, and 13% form the **C2** products in the (hot) electronic ground state. Importantly, the observations of Trentelman *et al.*¹⁵ suggest that the formation of the **C3** products is potentially a slow process as it requires intersystem crossing (ISC) onto the triplet manifold. However, the proposed photochemical mechanism assumes an S_1 intermediate that survives long enough to undergo thermalisation and, therefore, produce a statistical partitioning of products; this assumption does not necessarily hold given the speed at which $S_0 \leftarrow S_1$ relaxation is expected to take place. Kuhlman *et al.*^{11,27} have studied the 200 nm photolysis of cyclobutanone, comparatively, and reported conversion from the S_2 to the S_1 associated with two time constants of *ca.* 350 and *ca.* 750 fs. Using time-resolved mass spectrometry (TR-MS), the authors were able to resolve two fragments: the parent, and a fragment with a mass-to-charge ratio $m/z = 42$, corresponding to $H_2C-C=O$, both exhibiting similar electronically-excited-state decay

constants. The authors also reported a blue-shift in the photoelectron spectrum, arising from a coherent oscillatory motion assigned to a low frequency ring puckering mode with a frequency of 35 cm^{-1} , promoted by removal of an electron from an oxygen n orbital which leads to a relaxation of the sp^2 hybridization of the carbonyl carbon due to mixing with components of the bonding orbitals in the carbonyl group as well as a relaxation of the adjacent C-C bonds.

From the perspective of theory, Xia *et al.*¹⁷ performed a quantum chemistry investigation optimized minima, transition states, MECIs, and relaxed two-dimensional S_1 and T_1 potential energy surfaces using high-level quantum chemical calculations. On the basis of these calculations, Xia *et al.* proposed that ring opening predominately occurs in the S_1 state through an accessible S_1/S_0 MECI. Liu *et al.*¹⁸ extended this work by performing dynamics simulations within the *ab initio* multiple spawning (AIMS)^{28,29} framework following S_1 photoexcitation. They observed that relaxation occurred primarily through the S_1/S_0 MECI associated with fission of the first α -C-C bond, which fell into the region with the β -C-C bond is $\sim 1.6\text{ \AA}$, and the α -C-C bond between 2.5 - 3.5 \AA . In comparison they found that passage through intersections associated with the formation of the **C2** products, occurred when the β -C-C bond was around 4 \AA , but this constitutes only 15%. They reported an excited state lifetime in the S_1 state of *ca.* 500 fs and, on this basis, proposed that non-ergodic behavior was the driver of the change in **C3:C2** branching ratio as a function of excitation wavelength. In contrast, Kuhlman *et al.*²⁴ developed a four-state, five-dimensional model Hamiltonian and carried out quantum dynamics to study the $S_1 \leftarrow S_2$ relaxation dynamics. They concluded that $S_1 \leftarrow S_2$ relaxation involves specific nuclear modes included in the model Hamiltonian (including the cyclobutane ring-puckering, carbonyl out-of-plane deformation, symmetric and asymmetric C-CO-C stretches, and carbonyl stretching modes) that couple the S_2 and S_1 states and promote population transfer on the picosecond timescale. While informative, these potentials are built within a harmonic normal mode representation and are unable to address satisfactorily large amplitude nuclear motions associated with the formation of photoproducts.

Despite the concerted efforts of experiment and theory, there remain a significant number of open questions regarding the photochemistry and photochemical dynamics of cyclobutanone which evolve post-photoexcitation to the S_2 Rydberg ($3s \leftarrow n$) state. Nonetheless, the emergence of modern light sources^{30,31} is facilitating the study of ultrafast structural dynamics using both X-rays and electrons³²⁻³⁵ with ever-increasing spatial and temporal resolution and providing the potential for new and increasingly detailed insights into complex photochemical processes such as these. These developments are bringing into focus a crucial question (which is the focus of the

present Special Issue to which this Article contributes): *how accurate are modern nonadiabatic excited-state molecular dynamics simulations really?*

In this Article, we combine quantum- and excited-state trajectory surface-hopping molecular dynamics simulations at the LR-TDDFT(PBE0) and ADC(2) levels of theory to explore the relaxation dynamics of cyclobutanone post-photoexcitation to the S_2 Rydberg ($3s \leftarrow n$) state. Our excited-state molecular dynamics simulations are subsequently used predict the scattering signals for an ultrafast electron diffraction experiment in reciprocal and real space to establish how the complex photochemical dynamics of cyclobutanone might manifest as an experimental observable. In such an ultrafast electron diffraction experiment, free cyclobutanone molecules introduced *in vacuo* will be photoexcited at 200 nm [*i.e.* into the S_2 Rydberg ($3s \leftarrow n$) state] and probed *via* electron scattering at a sequence of temporal delays to image directly the evolving excited-state structural dynamics.

II. THEORY AND COMPUTATIONAL DETAILS

A. Quantum Chemistry

All quantum chemical calculations were carried out using Turbomole (v7.4).^{36,37} The quantum chemical calculations on the electronic ground and excited states used density functional theory (DFT) and linear-response time-dependent DFT (LR-TDDFT), respectively, with the PBE0 functional³⁸ and the aug-cc-pVDZ basis set.^{39,40} The Tamm-Dancoff⁴¹ approximation (TDA) was used throughout. Vibrational analysis were performed to confirm the absence of imaginary frequencies at the ground state minimum. Minimum-energy conical intersections (MECIs) were optimised at the LR-TDDFT(PBE0) level using Turbomole (v7.4) coupled with an external (penalty-function-based) optimiser.⁴² Linear reaction channels (produced *via* linear interpolation in internal coordinates; LIIC) between critical geometries and these CIs are available in the SI alongside benchmarks of the electronic structure and basis set.

Additional quantum chemical calculations were carried out at critical geometries using the second-order algebraic diagrammatic construction scheme [ADC(2)] and n -electron valence state perturbation theory (NEVPT2). All ADC(2) calculations were carried out using Turbomole (v7.4);^{36,37} all NEVPT2 calculations were carried out using ORCA.^{43,44}

B. Vibronic Coupling Hamiltonian and Quantum Dynamics

The model Hamiltonian developed is based upon the vibronic coupling approximation^{45,46} and is expressed as:

$$\mathbf{H} = (T_N + V_0)\mathbf{1} + \mathbf{W}^{dia.} + \mathbf{W}^{SOC} \quad (1)$$

The electronic diabatic Hamiltonian elements, $W_{n,n}$, are obtained by expanding $\mathbf{W} - V_0\mathbf{1}$ the diabatic potential as a Taylor series around a reference nuclear geometry, Q_0 , here taken as the Franck-Condon (*e.g.* S_0 minimum-energy) geometry. V_0 is a reference potential, here defined as a set of harmonic potentials with vibrational frequencies ω_i along dimensionless normal coordinates Q_i . In this case, the Hamiltonian elements are expressed as:

$$W_{n,m} - V_0\delta_{nm} = \epsilon_n\delta_{nm} + \sum_i^{3N-6} \left. \frac{\partial W_{n,m}}{\partial Q_i} \right|_{Q_0} Q_i + \frac{1}{2!} \sum_{i,j}^{3N-6} \left. \frac{\partial^2 W_{n,m}}{\partial Q_i \partial Q_j} \right|_{Q_0} Q_i Q_j + \frac{1}{3!} \left. \frac{\partial^3 W_{n,m}}{\partial Q_i \partial Q_j \partial Q_k} \right|_{Q_0} Q_i Q_j Q_k + \dots \quad (2)$$

where δ_{nm} is the Kronecker delta. Q_i denotes the $3N - 6$ dimensionless normal coordinates related to the normal modes of vibration where N is the number of atoms. V_0 , under the harmonic approximation, is expressed as:

$$V_0 = \frac{1}{2} \omega_i Q_i^2 \quad (3)$$

and the kinetic energy operator, \hat{T}_N , takes the form:

$$\hat{T}_N = - \sum_i \frac{1}{2} \omega_i \frac{\partial^2}{\partial Q_i^2} \quad (4)$$

Due to the anharmonicity of the potential energy surface, the Taylor series expansion is carried out up to fourth order.^{47,48} Obtaining the expansion coefficients for the Hamiltonian is simplified for the present system *via* use of symmetry; the minimum-energy S_0 geometry of cyclobutanone is C_s symmetric and, consequently, first- and second-order couplings are only allowed if the following selection rules are satisfied:

$$\Gamma_n \otimes \Gamma_{Q_a} \otimes \Gamma_n \supset A' \quad (5)$$

$$\Gamma_n \otimes \Gamma_{Q_a} \Gamma_{Q_b} \otimes \Gamma_n \supset A', \quad (6)$$

All expansion coefficients were obtained using a development version of the in-house-developed VCMaker^{49,50} software, available at Ref.⁵¹.

Quantum dynamics simulations over the multi-dimensional potential energy surface(s) were carried out using the multiconfigurational time-dependent Hartree (MCTDH)^{52,53} approach as implemented in Quantics.⁵⁴ The initial wavefunction for the electronic ground state was built using one-dimensional harmonic oscillator functions with zero initial momentum and vertically excited into the S_2 state at the Franck-Condon geometry ($Q = 0$). The complete computational details are provided in the SI and ensured convergence for the 2 ps of dynamics presented.

C. Excited-State Trajectory Surface-Hopping Molecular Dynamics

Ab initio excited-state trajectory surface-hopping molecular dynamics were performed using Newton-X (v2.4).^{55,56} The potential energy surfaces, derivatives, and respective couplings were computed on-the-fly using Turbomole (v7.4)^{36,37} at two separate levels of theory [LR-TDDFT(PBE0) and ADC(2)] in two separate sets of simulations. The trajectories were propagated using the velocity Verlet algorithm^{57,58} for a maximum of 5 ps ($t_{\text{max}} = 5000$ fs) with a time step of 0.5 fs ($dt = 0.5$ fs). The state-to-state transitions were simulated using the Hammes-Schiffer-and-Tully fewest-switches algorithm⁵⁹ with the state-to-state coupling estimated *via* the time-dependent Baer-An⁶⁰ coupling scheme. The excited-state trajectory surface-hopping molecular dynamics simulations were initiated by simulated vertical projection of a set of initial conditions, generated according to a Wigner distribution with a temperature of 100K, from the electronic ground state (S_0) into the S_2 Rydberg ($3s \leftarrow n$) state.

To avoid instabilities at/around the S_1/S_0 crossing seam, $S_0 \leftarrow S_1$ surface hops were forced when the S_1/S_0 energy gap fulfilled the criterion $\Delta E_{S_1-S_0} < 0.1$ eV.

D. Electron Diffraction Simulations

Throughout this work, we present the ultrafast electron diffraction scattering signal as a modified electron scattering intensity ($sM(s)$) as computed under the independent atom model (IAM). This presentation is used to enhance the oscillations in the scattering signal associated with the molecular interference terms and suppress the rapid drop-off in scattering signal intensity as a function of s from the elastic scattering amplitude. The modified electron scattering intensity is

given by:

$$sM(\mathbf{s}) = \frac{I_{\text{mol.}}(\mathbf{s})}{I_{\text{at.}}(\mathbf{s})} \mathbf{s} \quad (7)$$

where \mathbf{s} is the momentum transfer, or scattering, vector. $I_{\text{at.}}(\mathbf{s})$ is the atomic scattering term, given by:

$$I_{\text{at.}}(\mathbf{s}) = \sum_i^N |f_i(\mathbf{s})|^2 \quad (8)$$

and $I_{\text{mol.}}(\mathbf{s})$ is the molecular scattering term, expressed as a sum of interference terms, and given by:

$$I_{\text{mol.}}(\mathbf{s}) = \sum_i^N \sum_{j \neq i}^N |f_i(\mathbf{s})| |f_j(\mathbf{s})| \frac{\sin(\mathbf{s}r_{ij})}{\mathbf{s}r_{ij}} \quad (9)$$

where $f_i(\mathbf{s})$ and $f_j(\mathbf{s})$ are the elastic scattering amplitudes for atoms i and j , respectively, and r_{ij} is the internuclear distance between atoms i and j .

$sM(\mathbf{s})$ can be transformed into a pair-distribution function (PDF; *i.e.* from reciprocal space into real space) using a sine transform:

$$\text{PDF}(\mathbf{r}) = \int_0^{s_{\text{max}}} sM(\mathbf{s}) \sin(\mathbf{s}\mathbf{r}) e^{-ks^2} ds \quad (10)$$

where s_{max} is the maximum momentum transfer in the data, r is the internuclear distance between atom pairs, and k is a damping factor used to drive down smoothly the contribution(s) at high s to zero. A damping factor of $k = 0.03$ was used throughout.

The focus of this work is upon the ultrafast excited-state dynamics of cyclobutanone and, accordingly, the ultrafast electron diffraction scattering signal is presented as a transient (*i.e.* as an excited state — ground state 'difference') signal where appropriate under the nuclear ensemble model. The ground-state signal used to generate the transient is predicted from ground-state molecular dynamics, *i.e.* a nuclear ensemble of equilibrated configurations pre-photoexcitation. No scaling for, *e.g.*, excitation percentage/photolysis yield has been carried out.

III. RESULTS

A. Characterizing Critical Points on the Ground- and Electronically-Excited Potential Energy Surfaces

Table I shows the energies of the low-lying singlet (S_n ; $n = [1..5]$) and triplet (T_n ; $n = [1..5]$) electronically-excited states of cyclobutanone. Figure S1 shows the molecular orbitals involved in the electronic transitions. The symmetry point group of cyclobutanone (C_s at the S_0 minimum-energy geometry) is used to characterise the symmetries of the electronically-excited states (an important facet of the generation and interpretation of the model Hamiltonian used in the following section).

At the S_0 minimum-energy geometry, the S_1 and S_2 excited states are located 4.21 and 5.99 eV, respectively, above the electronic ground state at the ADC(2)/aug-cc-pVTZ level of theory, and at 4.33 and 6.10 eV, respectively, above the electronic ground state at the LR-TDDFT(PBE0)/aug-cc-pVTZ level of theory. Both levels of theory give good agreement with the experimental absorption spectrum recorded by Diau *et al.*,¹⁰ in which absorption bands are observed at *ca.* 4.2 and *ca.* 6.2 eV. At all levels of theory the S_1 and S_2 states have $\pi^* \leftarrow n$ (LUMO \leftarrow HOMO) and $3s \leftarrow n$ (LUMO+1 \leftarrow HOMO) character, respectively. The Rydberg character of the S_2 state requires a larger basis set to describe accurately its energy and electronic structure, while – in contrast – the valence S_1 state exhibits little to no dependence on the basis set (Table S1). Both the S_2 and S_1 states are of A'' symmetry; direct first-order vibronic coupling between these two states is consequently forbidden, and this can be expected to slow down the rate of internal conversion between the two states.

The ADC(2) calculations clearly give very good agreement with experimental observations at the Franck-Condon geometry. However, previous work has highlighted a limitation of this approach for studying non-radiative pathways of carbonyl-containing molecules⁶¹ as it predicts an artificial S_1/S_0 crossing along C=O vibrational arising from a $n \rightarrow \pi^*$ which is too shallow combined with a ground state which destabilises too rapidly. To address this, we calculate the potential along the C=O stretching normal mode, which is shown in Figure S2 calculated using LR-TDDFT(PBE0), ADC(2) and NEVPT2(12,12) levels of theory. This shows good agreement between the LR-TDDFT(PBE0) and NEVPT2(12,12) simulations, and although the ground state and S_1 surfaces become closer, they do not cross. In contrast, as expected from ref.⁶¹, there

is a clear crossing between the two surfaces in ADC(2), which corresponds to the C=O bond length of ~ 1.6 Å. This low lying accessible crossing point is likely to distort the excited state dynamics crossing from the S_1 to ground state surface and indeed such dynamics are presented in the supplementary material.

State	ADC(2)		LR-TDDFT(PBE0)	
	Energy / eV	Character (Irrep.)	Energy / eV	Character (Irrep.)
GS	0.00	— (A')	0.00	— (A')
S_1	4.21	H \rightarrow L (A'')	4.33	H \rightarrow L (A'')
S_2	5.99	H \rightarrow L+1 (A'')	6.10	H \rightarrow L+1 (A'')
S_3	6.53	H \rightarrow L+3 (A'')	6.67	H \rightarrow L+3 (A'')
S_4	6.64	H \rightarrow L+2 (A')	6.77	H \rightarrow L+2 (A')
S_5	6.68	H \rightarrow L+4 (A'')	6.78	H \rightarrow L+4 (A'')
T_1	3.87	H \rightarrow L (A'')	3.73	H \rightarrow L (A'')
T_2	5.95	H-1 \rightarrow L (A')	5.98	H-1 \rightarrow L (A')
		H-4 \rightarrow L		H-4 \rightarrow L
T_3	6.32	H \rightarrow L+1 (A'')	6.02	H \rightarrow L+1 (A'')
T_4	6.50	H \rightarrow L+3 (A'')	6.61	H \rightarrow L+3 (A'')
T_5	6.62	H \rightarrow L+2 (A')	6.63	H \rightarrow L+2 (A')

TABLE I. Summary of electronic energies, characters, and symmetries of the ground- (GS) and electronically-excited (S_n/T_n ; $n = [1..5]$) states of cyclobutanone evaluated at the S_0 minimum-energy geometry and at the ADC(2)/aug-cc-pVTZ and LR-TDDFT(PBE0)/aug-cc-pVDZ levels of theory. Comparative tables for evaluations at the S_1 - (Table S3) and S_2 -state (Table S4) minimum-energy geometries are presented in the SI. The relevant molecular orbitals are shown in the SI. The HOMO is designated as H; the LUMO is designated as L.

The S_1 state minimum-energy geometry is reached from the Franck-Condon point *via* an out-of-plane puckering and slight elongation of the C=O bond (1.21 to 1.26 Å); the C-C bonds in the cyclobutane ring remain almost unchanged. These structural changes destabilise the electronic ground state (Table S3); it is increased in energy by 1.13 eV relative to the S_0 minimum-energy geometry at the LR-TDDFT(PBE0)/aug-cc-pVDZ level of theory. In contrast, the S_1 ($\pi^* \leftarrow n$) state is stabilised, decreasing the energy gap with the S_0 state while increasing the gap with the

higher-lying singlet states (S_n ; $n > 1$). The predicted emission energy from the S_1 minimum-energy geometry is *ca.* 3.9 eV, a value that is in excellent agreement with the emission spectrum recorded by Lee *et al.*⁶² The broad band observed in the absorption spectrum recorded by Diau *et al.*¹⁰ is consistent with a short-lived electronically-excited state, however, which is indicative of competitive photochemical channels, *e.g.* non-radiative decay on the femto/picosecond timescale through accessible CIs as discussed by Liu *et al.*¹⁸

The S_2 state minimum energy geometry (Table S4), in contrast, is reached from the Franck-Condon point *via* contraction of the C=O bond (1.21 to 1.16 Å) and slight elongation of the C-C bonds in the cyclobutane ring. The largest influence on energy observed is a destabilisation of the ground state, which increases in energy by 0.51 eV with a similar (0.58 eV) increase observed for the S_1 state. The vibronic structure observed in the absorption spectrum for this state exhibits a distinct vibronic structure¹⁰ indicating both a longer lived excitation state and dominant vibrational modes activated upon excitation, which will be discussed in the following section.

Previous studies, *e.g.* Kao *et al.*,³ have hypothesised as to the potential role of triplet states in the photochemistry of cyclobutanone; this is our motivation for presenting these states (T_n ; $n = [1..5]$) in Table I and the relevant state-to-state spin-orbit couplings (SOCs) in the SI (Table S7). At the Franck-Condon geometry, the lowest-energy electronically-excited triplet state (T_1) is located at 3.73 eV above the electronic ground state at the LR-TDDFT(PBE0)/aug-cc-pVDZ level of theory and is of the same $\pi^* \leftarrow n$ character as the S_1 state; consequently, S_1/T_1 SOC will be formally forbidden.^{63,64} The T_2 and T_3 states are near-degenerate and located a little under the S_2 (6.10 eV) at 5.98 and 6.02 eV, respectively, above the electronic ground state at the LR-TDDFT(PBE0)/aug-cc-pVDZ level of theory. The SOC between these triplet states and the low-lying singlet electronically-excited states is generally small (Table S7), suggesting that the triplet states are unlikely to play a significant role in the early-time (*e.g.* <2 ps) photochemistry focused upon in the present work.

Figure 2b shows the structure of an S_2/S_1 MECI, while Figures 2c-e show the structures of three S_1/S_0 MECI. Cartesian coordinates are given in the SI. Potential energy surface(s) between the Franck-Condon point and each of the S_1/S_0 MECI were calculated *via* linear interpolation in internal coordinates (LIIC) at the LR-TDDFT(PBE0) level are also given in the SI.

The S_2/S_1 MECI (Figure 2b) is located at 5.85 eV above the S_0 minimum-energy geometry, *i.e.* *ca.* 0.5 eV below the $3s \leftarrow n$ excitation energy, at the LR-TDDFT(PBE0)/aug-cc-pVDZ level of theory. Its structure is similar to the Franck-Condon geometry although it features a symmetry-

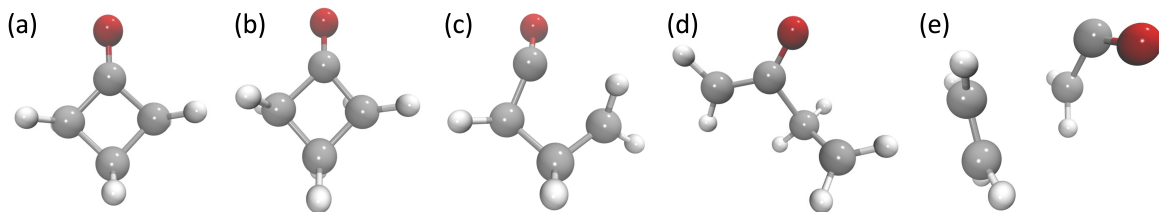


FIG. 2. Key geometries of cyclobutanone: (a) the S_0 minimum-energy geometry, (b) the (symmetry-broken) S_2/S_1 MECI, and the S_1/S_0 (c) C_α -cleavage, (d) C_β -cleavage, and (e) concerted C_α -/ C_β -cleavage MECIs. All geometries were optimised at the LR-TDDFT(PBE0)/aug-cc-pVDZ level of theory.

breaking distortion of the cyclobutane ring (seen clearly on inspection of the position of the hydrogen atoms in Figure 2b). The potential energy surface between the Franck-Condon geometry and this S_2/S_1 MECI is barrierless (Figure S3) which would suggest that S_2/S_1 internal conversion should be (ultra)fast in the absence of any additional considerations, however the symmetry of the two states at the Franck-Condon geometry is such that the interstate coupling is forbidden; even at the distorted S_2/S_1 MECI geometry, it is weak and results in a predictably longer lifetime for the S_2 state.

The three S_1/S_0 MECI (Figure 2c-e) obtained are in close qualitative agreement (geometrically and energetically) with those located at the CASPT2 level of theory and reported in Ref.¹⁸. The first is located along the α -cleavage channel, the second along the β -cleavage channel, and the third along a concerted α/β -cleavage channel. The energetic ordering of the three S_1/S_0 MECIs (3.40, 2.56 and 5.0 eV, respectively, above the S_0 minimum-energy geometry at the LR-TDDFT(PBE0)/aug-cc-pVDZ level of theory) follows qualitatively the trend observed for the three S_1/S_0 MECIs in Ref.¹⁸, although it is important to note that the single-reference nature of LR-TDDFT(PBE0) favours charged rather than biradical dissociation along the α - and β -cleavage channels and, furthermore, renders it unable to describe properly the topology/dimensionality of the S_1/S_0 crossing seam. Although all of the S_1/S_0 MECIs are energetically accessible (*i.e.* they and their barriers are submerged relative to the *ca.* 6.2 eV excitation energy, the description of the potential energy surface around the S_1/S_0 MECIs is likely to be problematic for LR-TDDFT(PBE0) and it is quite possible that this might influence the photoproduct production by influencing the internal conversion dynamics through the MECI and, subsequently, the motion of the trajectory/wavepacket on the electronic ground state potential energy surface.

Overcoming these aforementioned limitations could be achieved using a multireference (active

space) method, *e.g.* CASSCF/CASPT2 or NEVPT2, for the excited-state molecular dynamics simulations. However, the performance of these methods is greatly dependent on the choice of active space; an appropriate active space should be large enough to incorporate all of the orbitals required over all of the nuclear configurations explored in the excited-state molecular dynamics simulations while not too large so as to render the simulations computationally costly to the point of intractability. We found an active space of eight electrons in eight orbitals [*e.g.* NEVPT2(8,8)] unstable with respect to orbital rotation(s) at some distorted cyclobutane geometries, while a larger active space of twelve electrons in twelve orbitals [*e.g.* NEVPT2(12,12)] was too computationally expensive to carry out practicably excited-state molecular dynamics simulations. Consequently, in the present work, we have carried out our excited-state molecular dynamics simulations using LR-TDDFT(PBE0) and ADC(2), keeping in mind the aforementioned (although well-understood) limitations and their potential impact on the dynamics (which we discuss in detail). However, we note within the context of the present challenge, other contributors have performed excited-state molecular dynamics simulations with CASSCF based on an eight-electron-in-eleven-orbital active space⁶⁵ and extended multistate CASPT2 (XMS-CASPT2) based on an eight-electron-in-eight-orbital active space.⁶⁶

B. Early-Time Dynamics Using a Spin-Vibronic Coupling Hamiltonian

To i) identify possible photochemical (fragmentation) channels, ii) clarify the potential involvement of triplet states, and iii) establish a mechanism for internal conversion from the initially-excited S_2 ($3s \leftarrow n$) state to the lowest-energy singlet electronically-excited state (S_1) at early times, we employ a model Hamiltonian and carry out quantum dynamics simulations as described above. The model Hamiltonian comprises the electronic ground state (S_0) and nine electronically-excited states [four singlets (S_n ; $n = [1..4]$) and five triplets (T_n ; $n = [1..5]$)]. The inclusion of singlet states higher in energy than the S_2 (*e.g.* S_n ; $n > 2$) is motivated by the absence of vibronic coupling between the S_1 and S_2 states, both of which are of A'' symmetry (Table I); here, coupling to higher-lying singlet states of, *e.g.*, alternative symmetries offers the potential of second-order population transfer channels comparable to those identified in other systems where direct population transfer channels are weak or otherwise absent.^{67–69}

In nuclear configurational space, the model Hamiltonian incorporates eight degrees of vibrational freedom: ν_1 , ν_7 , ν_{10} , ν_{11} , ν_{12} , ν_{13} , ν_{15} , and ν_{21} , which were identified by the magnitude of

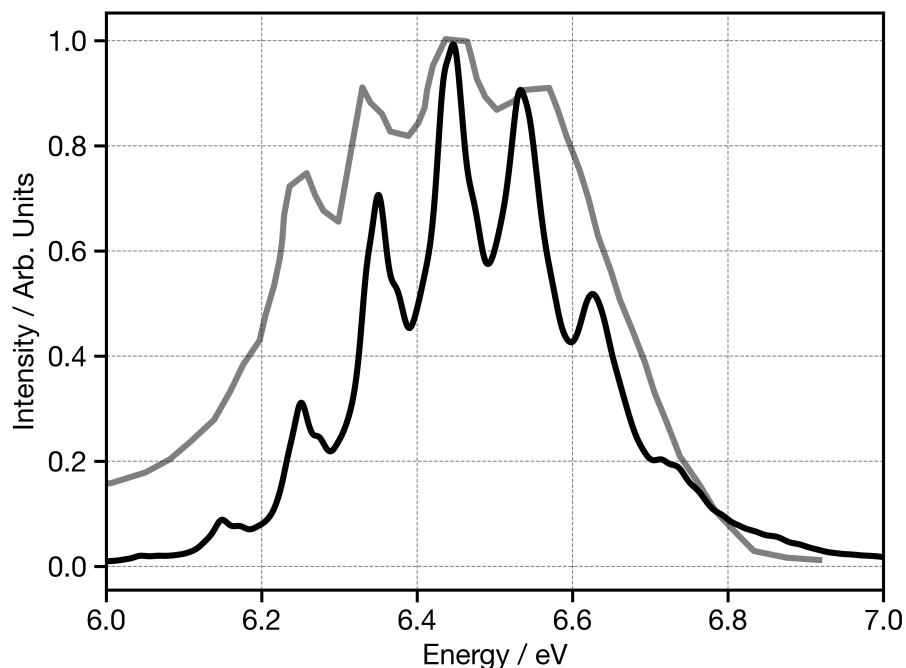


FIG. 3. Theoretical (black) and experimental (grey) $S_2 \leftarrow S_0$ ($3s \leftarrow n$) absorption spectrum. The theoretical spectrum is shown shifted by $\Delta E = +0.14$ eV. The experimental spectrum was recorded by Diau *et al.* and digitised from Ref.¹⁰

their first-order couplings and the symmetries of the vibrational modes. The degrees of vibrational freedom included the model Hamiltonian comprise cyclobutane ring puckering (ν_1 and ν_{12}), symmetric and anti-symmetric cyclobutane ring breathing (ν_7 and ν_{10}), cyclobutane ring deformation (ν_{11} , ν_{13} and ν_{15}), and the C=O stretching mode (ν_{21}), consistent with previous works.¹¹ To assess the approximate accuracy of our model Hamiltonian, Figure 3 compares the experimental¹⁰ and theoretical absorption spectrum for the S_2 state. There is excellent agreement between the two, indicating that our model Hamiltonian describes accurately the (local) potential energy surface(s). The absorption spectrum features a distinct vibrational progression with structured peaks separated by *ca.* 0.1 eV consistent with the C=O out-of-plane wagging and cyclobutane ring puckering vibrational modes previously identified⁷⁰ and arising in the present model *via* the inclusion of ν_{12} .

Figure 4 shows the transfer of population from the S_2 state over 600 fs post-photoexcitation into the S_2 ($3s \leftarrow n$) state as computed *via* quantum dynamics. The $S_1 \leftarrow S_2$ population transfer occurs at a rate of *ca.* $1.67 \times 10^{-12} \text{ s}^{-1}$ with the S_1 state reaching peak population within *ca.* 350 fs and is qualitatively consistent with the decay of the peak associated with the S_2 state in the pho-

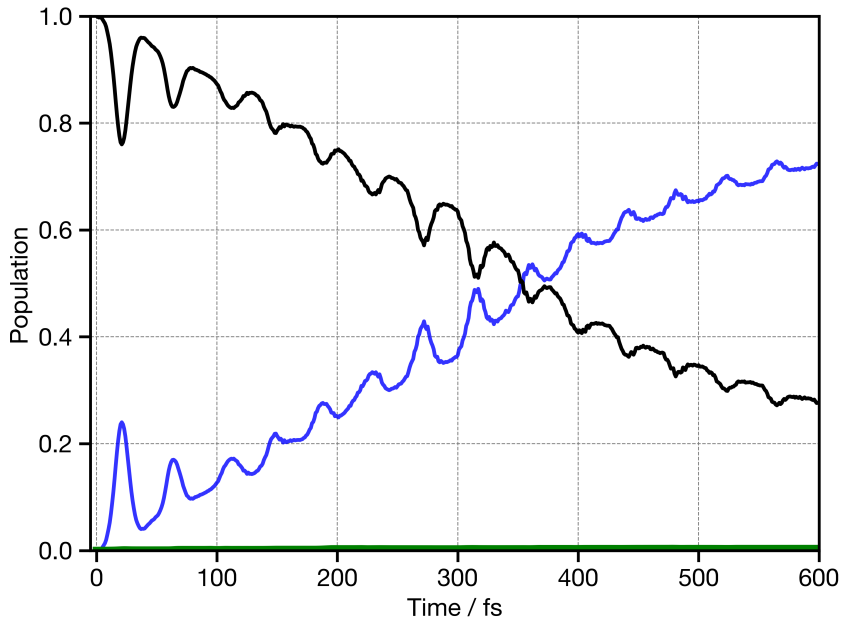


FIG. 4. Population kinetics obtained from quantum dynamics simulations over 600 fs post-photoexcitation into the S_2 ($3s \leftarrow n$) state. The S_2 state population is shown in black; the S_1 state population is shown in blue; the triplet (T_n ; $n = [1..5]$) state populations are shown (collectively) in green.

toelectron spectrum recorded by Kuhlman *et al.*¹¹ (the authors report a biexponential fit yielding time constants of *ca.* 350 and 750 fs). The $S_1 \leftarrow S_2$ population transfer in the model Hamiltonian obtains intensity *via* mixing with the higher-lying singlet electronically-excited states, especially the S_4 state (the lowest-lying singlet electronically-excited state of A' character). This occurs most prominently along ν_{11} . While this mode is responsible for the state-to-state coupling, it is ν_1 , ν_{12} , ν_{13} , and ν_{21} which exhibit the largest-amplitude nuclear oscillations and electronically-excited-state structural changes which are likely to be observed in the ultrafast electron diffraction experiment. The population oscillations observed between the S_2 and S_1 states are associated with the overcoherence of the reduced model Hamiltonian and are, in any case, faster than the temporal resolution of the ultrafast electron diffraction experiments.

$S_0 \leftarrow S_1$ population transfer is not included in the present model Hamiltonian. The high energy of the S_2 state results in an exceptionally hot wavefunction on the electronic ground state that is difficult to converge under the framework of the quantum dynamics simulations. In addition, previous works – and our own quantum chemical calculations – have identified S_1/S_0 MECI at highly distorted geometries beyond the limits of the normal model representation on which the quantum

dynamics simulations are predicated (the representation is only valid to small distortions from the equilibrium, *e.g.* S_0 minimum-energy, geometry). Consequently, to describe more completely the excited-state relaxation dynamics, we explore excited-state molecular dynamics simulations operating in unconstrained nuclear configurational space through the trajectory surface-hopping approach.

C. Excited-State Relaxation Dynamics in Unconstrained Nuclear Configuration Space Using Trajectory Surface-Hopping Dynamics

Figure 5 shows the populations of the S_2 , S_1 and S_0 states over the first 2 ps post-photoexcitation into the S_2 ($3s \leftarrow n$) state as obtained from 289 *on-the-fly* surface-hopping trajectories propagated at LR-TDDFT(PBE0)/aug-cc-pVDZ level of theory. A similar set of trajectory surface-hopping dynamics propagated at the ADC(2)/aug-cc-pVDZ level of theory are presented and analysed in the SI and are of comparative interest.

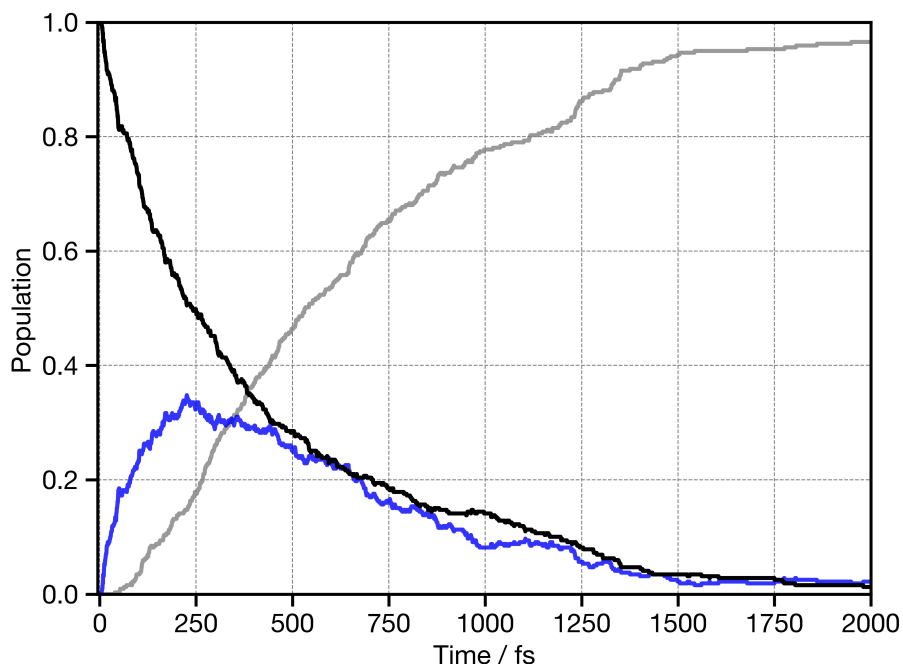


FIG. 5. Population kinetics obtained from 289 *on-the-fly* surface-hopping trajectories over 2 ps post-photoexcitation into the S_2 ($3s \leftarrow n$) state. The S_2 state population is shown in black; the S_1 state population is shown in blue; the S_0 state population is shown in gray.

Figure 5 shows $S_1 \leftarrow S_2$ population transfer with a decay constant of *ca.* 356 fs. This is

slightly faster than observed in the quantum dynamics simulations, *i.e.* 50% of population decays from S_2 in 225 fs, which is due to the inclusion of the ground state to which the wavepacket can rapidly decay. This decay constant is in close agreement with the fastest time-constant extracted from a photoelectron spectroscopic study,¹¹ but we do not see any dynamics associated with the ~ 700 fs component reported. Interestingly, this slower component is in close agreement with the population kinetics for the dynamics performed using potentials calculated at ADC(2) level of theory, shown in the supporting information.

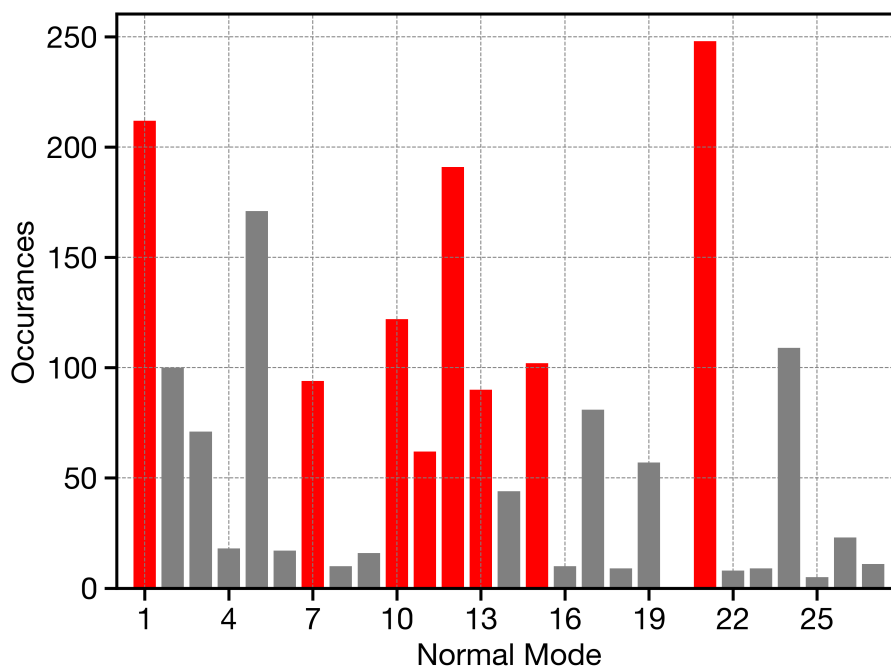


FIG. 6. Bar chart showing the the number of times that each normal mode features in the top six largest displacements for an (electronically-excited-state) trajectory. The red bars represent those normal modes included in the model Hamiltonian.

While the time scales between the quantum dynamics and TSH simulations suggests similar dynamics, further analysis is required to assess this in more detail. To achieve this, we transform the first 500 fs of excited state molecular dynamics from Cartesian coordinates into a normal mode representation similar to ref.⁷¹. Figure 6 shows the normal modes active during the TSH simulations as a bar chart of the number of times each normal mode features in the top 6 of the largest displacements during a trajectories excited state dynamics. The red bars represent those normal modes included in the model Hamiltonian. This shows close agreement between the modes which appear most frequently in the TSH simulations and those included in the quantum

dynamics. The most notable exception is ν_5 which exhibits larger amplitude motion due to the flat nature of the potential, but does not act as either tuning or coupling modes and therefore do not strongly influence the excited state dynamics.

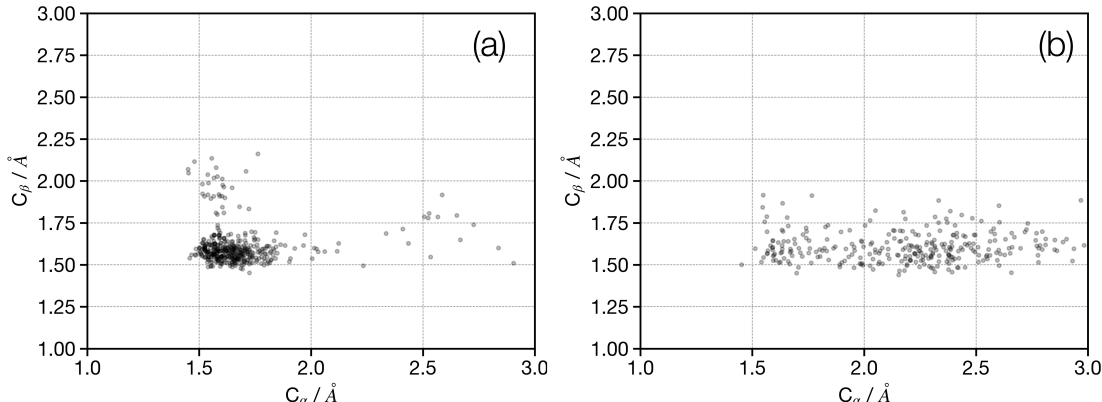


FIG. 7. Average C_α and C_β bond lengths at (a) $S_1 \leftarrow S_2$ and (b) $S_0 \leftarrow S_1$ surface-hopping events.

Figure 7 shows average C_α and C_β bond lengths for the structures where each trajectory hops from the S_2 - S_1 (a) and S_1 - S_0 (b) states. For the former, there is a clear cluster around 1.5-1.6 Å consistent with the ground state structure and therefore close to the Franck-Condon geometry, as expected from the optimised S_2/S_1 discussed above. In contrast, for the S_1 - S_0 hopping geometries, there is a significant change, with the majority of hops occurring for C_α bond lengths >2.2 Å. Using the geometries provided in the supporting information, the C_α CI occurs when the C_α bond length is 2.35 Å, with very little correspond change along the C_β bond. This suggests, in agreement with previous work, that crossing from the S_1 - S_0 occurs primarily at the CI exhibiting a C_α bond break.

Figure 8 shows the fractional population of the photoproducts formed from the TSH trajectories. This indicates $\sim 20\%$ of the excited states form the $C_2H_4 + CH_2CO$, *i.e.* decay *via* the **C2** channel, while 2.5% forms the **C3** products. The ring-open species are formed, but are very short-lived and either contribute forming either the **C2** or **C3** products or undergo bond reformation to form vibrationally excited ground state cyclobutanone. The formation of **C2** comparable, but lower than other excited state dynamics simulations performed at a higher level of theory reported in ref.⁶⁶ (34%) and with Trentelman *et al.*¹⁵ who reported 43% of yield experimentally. The major discrepancy in our simulations occurs for the **C3** channels, which is $>60\%$ in these previous works. The near-absence of the **C3** channel is associated with the multi-reference character of the

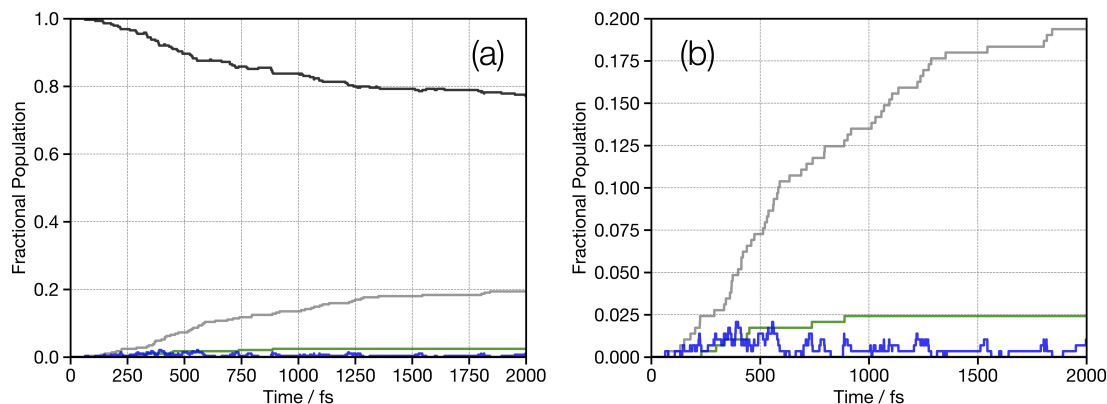


FIG. 8. Fractional population of the photoproducts obtained from the 289 trajectories. The black trace shows cyclobutanone, the grey trace shows the **C2** products ($\text{C}_2\text{H}_4 + \text{CH}_2\text{CO}$), the green trace shows the **C3** products ($\text{C}_3\text{H}_6 + \text{CO}$), and the blue trace shows ring-opened structures.

potential in this region and the bias of single reference methods for charged rather than biradical bond breaking. While this does not significantly increase the energies of the C_α and C_β CIs (see Figure S4), it does increase the energy of the double bond breaking CI, making the formation of the **C3** channel challenging. To assess this we also perform dynamics using trajectories in the T_1 state, performed using unrestricted Kohn-Sham facilitating the description of biradical character. These were initiated at random from trajectories populating the S_1 state. Importantly, these show a much higher formation of **C3** photoproducts (**C3**: 53%, **C2**: 5% and ring-open: 17%) consistent with previous experiments¹⁵.

D. Electron Diffraction Simulations

Figure 9 shows the time resolved electron diffraction simulations arising after photoexcitation of cyclobutanone into the S_2 state. Figure 9a show the electron diffraction scattering signal as calculated, while Figure 9b is convolved along the temporal axis with a Gaussian kernel (FWHM = 150 fs) to reproduce the effect(s) of the finite temporal resolution of the proposed electron diffraction experiment. Figures 9c and d show time-resolved pair-distribution function (PDFs) maps with and without temporal broadening, respectively, and were produced *via* sine transformation of the modified scattering intensity maps in Figures 9a and b, respectively.

The modified scattering intensity maps (Figures 9a and b) show two strong negative (*ca.* 1 and 9 \AA^{-1}) and two positive (*ca.* 2.7 and 7.5 \AA^{-1}) features but do not reveal the richness of the dynamics

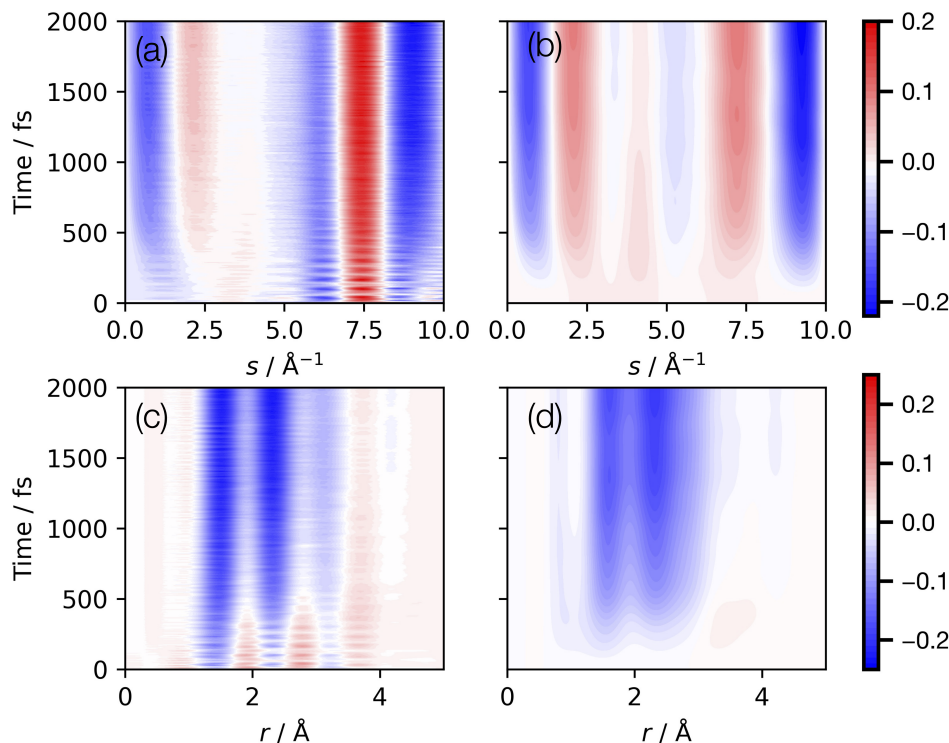


FIG. 9. Transient ($\Delta I/I$) scattering (a) without and (b) with 150 fs (FWHM) temporal broadening. Transient PDF (c) without and (d) with 150 fs (FWHM) temporal broadening. The ground-state (pre-photoexcitation) signal used to generate the transient signal was obtained from the trajectory surface-hopping dynamics initial conditions, *i.e.* the nuclear ensemble representing the state of the system at $t = 0$. All plots were produced using the 289 2000-fs trajectories simulated at the LR-TDDFT(PBE0)/aug-cc-pVDZ level of theory.

that reflect the complex photochemistry of cyclobutanone, in part due to the incoherent/stochastic nature of the photochemical processes taking place.

A deeper understanding of the structural changes can be established from Figures 9c and d, which show the time-resolved PDF. For clarity, Figure 10 shows the PDF($t = 0$ fs), PDF($t = 2000$ fs), and the Δ PDF($t = 2000$ fs). The PDF acquired for the 289 initial conditions exhibits 3 peaks at ~ 1.5 Å, ~ 2.5 Å and ~ 3.0 Å. The first corresponds to the neighboring C-C and C=O distances, the second corresponds to C-C distance on the opposite side of the cycle and the final peak corresponds to the C-O distances which are not directly bonded. The transient indicates primarily a loss of the first two peaks associated with dissociation and the formation of the **C2** products. We note here

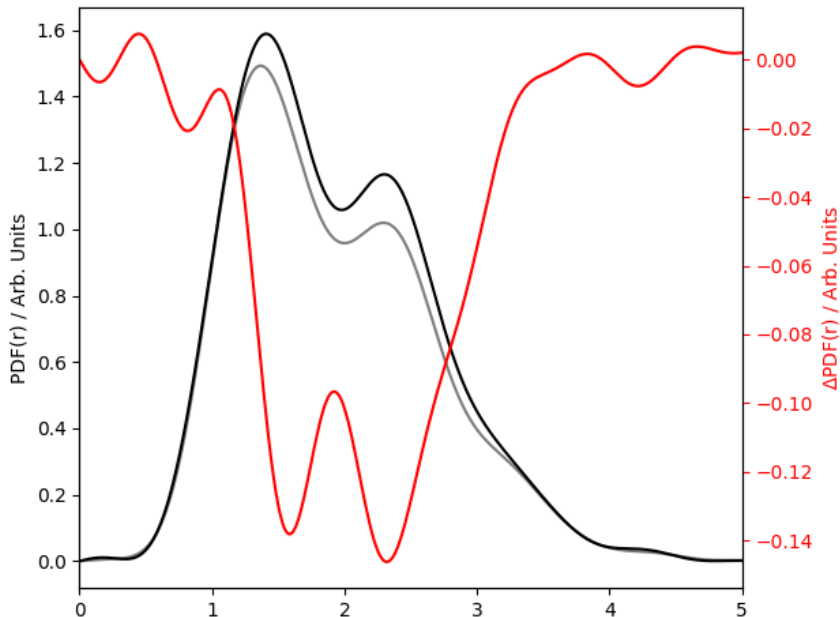


FIG. 10. Initial ($t = 0$ fs; black) and final ($t = 2000$ fs; grey) PDFs and the difference PDF (red) calculated using the 289 2000 fs surface hopping trajectories simulated using potentials are LR-TDDFT(PBE0) level of theory.

that despite the aforementioned differences in the photoproduct formation, the transient scattering and PDFs are very similar to those in ref.⁶⁶. This highlights the challenge in disentangling the exact photoproduct formation of these systems due to the overlapping bands.

IV. DISCUSSION AND CONCLUSIONS

In this work, we have carried out quantum and excited-state trajectory surface-hopping molecular dynamics simulations to study the electronically-excited-state relaxation mechanisms and electronic ground-state dynamics of cyclobutanone post-photoexcitation into the S_2 Rydberg ($3s \leftarrow n$) state. Our focus has been upon translating these simulations to predict the experimental observables associated with the ultrafast electron diffraction experiments and ultimately to answer the question: *Can excited state dynamics simulations be predictive?* However, even for small molecules such as cyclobutanone, certain approximations in the underlying computational chemical methods are required which will influence the outcome of such simulations: we highlight this in comparison between the present work and other works related to the same challenge.^{65,66,72,73} Consequently, in this section we discuss the relaxation mechanism observed in our simulations as

well as potential sources of error and how we expect that these will influence interpretation of the experimental observables.

Within this challenge, the objective has been to translate excited state dynamics into experimental observables. The importance of this cannot be understated. In many cases, collaboration between experimental and theoretical studies focus upon the comparison of quantities that are easy to calculate, such as electronic state population kinetics. These kinetics are then compared to experimentally extracted timescales and agreement is taken as accuracy of the simulations. However, as shown in this work the LR-TDDFT (356 fs) and XMS-CASPT2⁶⁶ (335 fs) dynamics provide very similar decay kinetics, but different predictions of photoproducts which would influence the experimental signal. While slightly slower, the excited state dynamics performed using ADC(2) potentials also occurs on a comparable timescale (~ 700 fs), but owing to the artificial crossing along the C=O bond stretch⁶¹, the excited state decay occurs via a completely different mechanism.

Our simulations indicate that after excitation of the $3s \leftarrow n$ Rydberg state the system relaxes within 1-2 ps to form a broad range of photoproducts. Decay of this initially excited S_2 state occurs with a time-constant of ~ 350 fs. This is in good agreement with the fastest kinetics reported from previous time-resolved photoelectron experiments by Kuhlman *et al.*¹¹. However, we note that ref.¹¹ also reports a strong contribution from a slower time component, ~ 750 fs. This is not observed within the LR-TDDFT population kinetics, but is in very close agreement with the ADC(2) kinetics presented in the supporting information. The exact origin for this difference between LR-TDDFT and ADC(2) is unclear, however analysis of the *hopping* geometries, indicates a flatter potential in the case of the latter, which permits a slightly wider spread of the trajectories in nuclear configuration space. Importantly, in both cases despite the small nuclear displacement required to reach the crossing point, the internal conversion from S_2 to S_1 is comparatively slow due to the symmetry forbidden nature of the transition.

Once populated, the S_1 undergoes a large structural distortion, primarily along the C_α bond, consistent with previous work^{10,18}. This drives population to be rapidly transferred into the electronic ground state to form very vibrationally hot species. The fast nature of the population transfer from the S_1 to the ground state means that population of the S_1 doesn't exceed $\sim 30\%$. The excited state molecular dynamics consider only the dynamics within the singlet manifold. To assess the potential influence of the intersystem crossing and the triplet states, our quantum dynamics include the low lying excited triplet states. These simulations indicate negligible amount of intersystem

crossing into the triplet manifold leading us to conclude that this channel will be unable to compete with internal conversion rates found here.

Although the excited state dynamics and high energy of excitation leads to some highly distorted geometries, our simulations point to the formation of the photoproducts being determined as the trajectory passes through the CI between the first electronically excited state and the ground state *via* a ring-opened intermediate. This is consistent with the conclusions from ref.¹⁰ who demonstrated that motion away from the CI branching space leads to all of the observed photoproducts. Herein lies the most significant approximation within our work, as neither of the single reference method used will capture the biradical nature of the photoproducts. Indeed, although all of the CI identified¹⁸ in previous work have been found within the LR-TDDFT(PBE0) framework and exist at accessible energies, *i.e.* below the excitation energy, our simulations show a much lower fraction of photoproduct formation than previous theoretical^{65,66,72,73} and experimental¹⁵ works. This appears to most strongly affect the **C3** photoproducts, which only forms in 2.5% of the trajectories. In contrast, trajectories in the T_1 state, performed using unrestricted Kohn-Sham facilitating the description of biradical character, initiated at random from trajectories populating the S_1 state, show a much higher formation of **C3** photoproducts (**C3**: 53%, **C2**: 5% and ring-open: 17%) consistent with previous experiments¹⁵. The motion through the CI and therefore the potential shape in this region is likely to be critical in determining the branching ratio of the photoproducts. Here it may not only be a limitation of single reference methods but a also condition of the excited state dynamics used. As stated in the methods section, our present dynamics attempts to avoid instabilities in the multi-configurational region, near the degeneracy by enforcing a hop to the ground state when the S_1 - S_0 energy gap became $\Delta E_{S_1-S_0} < 0.1\text{eV}$. While this avoids the explicit motion through the CI, the enforced earlier transition may also promote populated transfer closer the cyclobutanone structure encouraging reformation of vibrationally hot cyclobutanone, rather than the photoproducts.

From these excited state molecular dynamics simulations, the ultrafast electron diffraction observable shows distinct changes and by studying the time-resolved PDF, these are largely associated with a loss in intensity for interactions at 1.5 and 2.5 Å, arising from dissociation. Despite the rich dynamics and the distinct changes observed, the time-resolved scattering curves show very little distinct dynamics largely associated with the incoherent nature of the dynamics and the comparatively low temporal resolution (150 fs).

Finally, a logical question would be ask if the limitations discussed above can be overcome

within the present framework, *i.e.* without adopting a multi-reference wavefunction method which would prove challenging for larger systems. Here, it is important to stress that while the relative yields of photoproducts formed appears somewhat at odds with previous works, all major reported products are generated, *i.e.* the full nuclear configuration space has been sampled. Excited state simulations have previously been used to simulate the experimental observables associated with structurally sensitive techniques of electron⁷⁴ and X-ray diffraction³⁵. Importantly in both of these works the outcomes of the trajectory-based dynamics were used as a basis to fit to experimental data and deliver an interpretation. While, the use of a fit means that such an approach may not be classed as fully predictive, in both cases an excellent agreement between experiment and theory was achieved and providing deep insight into the dynamics observed.

ACKNOWLEDGEMENTS

This research made use of the Rocket High Performance Computing service at Newcastle University and the Viking High Performance Computing service at the University of York. We also acknowledge the COSMOS Programme Grant (EP/X026973/1). T. J. P would like to thank the EPSRC for an Open Fellowship (EP/W008009/1).

REFERENCES

- ¹R. Norrish and C. Bamford, "Photodecomposition of aldehydes and ketones," *Nature* **138**, 1016–1016 (1936).
- ²N. J. Turro, J. C. Dalton, K. Dawes, G. Farrington, R. Hautala, D. Morton, M. Niemczyk, and N. Schore, "Molecular photochemistry. I. molecular photochemistry of alkanones in solution.. alpha.-cleavage, hydrogen abstraction, cycloaddition, and sensitization reactions," *Accounts of Chemical Research* **5**, 92–101 (1972).
- ³M.-H. Kao, R. K. Venkatraman, M. N. Ashfold, and A. J. Orr-Ewing, "Effects of ring strain on the ultrafast photochemistry of cyclic ketones," *Chemical Science* **11**, 1991–2000 (2020).
- ⁴H. Denschlag and E. K. Lee, "On the mechanism of the photochemical decomposition of cyclobutanone in the gas phase," *Journal of the American Chemical Society* **89**, 4795–4797 (1967).
- ⁵R. J. Campbell and E. W. Schlag, "Energy distribution in reaction products. photolysis of cyclobutanone," *Journal of the American Chemical Society* **89**, 5103–5106 (1967).

- ⁶D. R. Morton and N. J. Turro, "Photochemical ring expansion of cyclic aliphatic ketones. cyclobutanones and cyclopentanones," *Journal of the American Chemical Society* **95**, 3947–3957 (1973).
- ⁷J. C. Hemminger and E. K. Lee, "Fluorescence excitation and photodecomposition of the first excited singlet cyclobutanone (1 a 2): A study of predissociation of and collisional energy transfer from the vibronically selected species," *The Journal of Chemical Physics* **56**, 5284–5295 (1972).
- ⁸N. E. Lee and E. K. Lee, "Tracer study of photochemically excited cyclobutanone-2-t and cyclobutanone. ii. detailed mechanism, energetics, unimolecular decomposition rates, and intermolecular vibrational energy transfer," *The Journal of Chemical Physics* **50**, 2094–2107 (1969).
- ⁹N. J. Turro and R. M. Southam, "Molecular photochemistry. iv. solution photochemistry of cyclobutanone and some derivatives," *Tetrahedron Letters* **8**, 545–551 (1967).
- ¹⁰E. W.-G. Diau, C. Kötting, and A. H. Zewail, "Femtochemistry of norrish type-i reactions: Ii. the anomalous predissociation dynamics of cyclobutanone on the s1 surface," *ChemPhysChem* **2**, 294–309 (2001).
- ¹¹T. S. Kuhlman, T. I. Sølling, and K. B. Møller, "Coherent motion reveals non-ergodic nature of internal conversion between excited states," *ChemPhysChem* **13**, 820–827 (2012).
- ¹²J. Zhang, W.-Y. Chiang, and J. Laane, "Jet-cooled fluorescence excitation spectra and carbonyl wagging and ring-puckering potential energy functions of cyclobutanone and its 2, 2, 4, 4-d 4 isotopomer in the s1 (n, π^*) electronic excited state," *The Journal of Chemical Physics* **100**, 3455–3462 (1994).
- ¹³E. K. Lee, J. C. Hemminger, and C. F. Rusbult, "Unusual photochemistry of cyclobutanone near its predissociation threshold," *Journal of the American Chemical Society* **93**, 1867–1871 (1971).
- ¹⁴R. F. Whitlock and A. Duncan, "Electronic spectrum of cyclobutanone," *The Journal of Chemical Physics* **55**, 218–224 (1971).
- ¹⁵K. A. Trentelman, D. B. Moss, S. H. Kable, and P. L. Houston, "The 193-nm photodissociation of cyclobutanone: Dynamics of the c2 and c3 channels," *Journal of Physical Chemistry* **94**, 3031–3039 (1990).
- ¹⁶M. Larsen, A. Stephansen, and T. Sølling, "Coherent motion of excited state cyclic ketones: The have- and the have-nots," *Chemical Physics Letters* **683**, 495–499 (2017).
- ¹⁷S.-H. Xia, X.-Y. Liu, Q. Fang, and G. Cui, "Excited-state ring-opening mechanism of cyclic ketones: An ms-caspt2//casscf study," *The Journal of Physical Chemistry A* **119**, 3569–3576

- (2015).
- ¹⁸L. Liu and W.-H. Fang, “New insights into the photodissociation dynamics of cyclobutanone from aims dynamic simulation,” *The Journal of Chemical Physics* **144** (2016).
- ¹⁹A. Hopkinson, E. Lee-Ruff, and H. Lien, “Molecular orbital calculations of excited state cyclobutanone and its photocarbene,” *Tetrahedron* **44**, 6815–6820 (1988).
- ²⁰F. Momicchioli, I. Baraldi, and G. Di Lonardo, “Structure of the b state of cyclobutanone,” *Journal of the Chemical Society, Faraday Transactions 2: Molecular and Chemical Physics* **71**, 791–798 (1975).
- ²¹J. Dalton and N. Turro, “Photoreactivity of n , π^* excited states of alkyl ketones,” *Annual Review of Physical Chemistry* **21**, 499–560 (1970).
- ²²Y. Chen and S. Ye, “Photochemical reaction mechanism of cyclobutanone: A casscf study,” *International Journal of Quantum Chemistry* **97**, 725–735 (2004).
- ²³T. S. Kuhlman, S. Sauer, T. I. Sølling, and K. B. Møller, “Symmetry, vibrational energy redistribution, and vibronic coupling: The internal conversion processes of cycloketones,” *The Journal of Chemical Physics* **137** (2012).
- ²⁴T. Kuhlman, S. P. Sauer, T. Sølling, and K. B. Møller, “Quantum-dynamical modeling of the rydberg to valence excited-state internal conversion in cyclobutanone and cyclopentanone,” in *EPJ Web of Conferences*, Vol. 41 (EDP Sciences, 2013) p. 02033.
- ²⁵G. M. Breuer and E. K. Lee, “Fluorescence decay times of cyclic ketones, acetone, and butanal in the gas phase,” *The Journal of Physical Chemistry* **75**, 989–990 (1971).
- ²⁶K. Y. Tang and E. K. Lee, “Laser photolysis of cyclobutanone. photodecomposition from selected vibronic levels at long wavelengths,” *The Journal of Physical Chemistry* **80**, 1833–1836 (1976).
- ²⁷T. S. Kuhlman, M. Pittelkow, T. I. Sølling, and K. B. Møller, “Pulling the levers of photophysics: How structure controls the rate of energy dissipation,” *Angew. Chem., Int. Ed* **52**, 2247–2250 (2013).
- ²⁸M. Ben-Nun, J. Quenneville, and T. J. Martínez, “Ab initio multiple spawning: Photochemistry from first principles quantum molecular dynamics,” *The Journal of Physical Chemistry A* **104**, 5161–5175 (2000).
- ²⁹B. F. Curchod and T. J. Martínez, “Ab initio nonadiabatic quantum molecular dynamics,” *Chemical Reviews* **118**, 3305–3336 (2018).

- ³⁰D. Filippetto, P. Musumeci, R. Li, B. J. Siwick, M. Otto, M. Centurion, and J. Nunes, “Ultrafast electron diffraction: Visualizing dynamic states of matter,” *Reviews of Modern Physics* **94**, 045004 (2022).
- ³¹C. Pellegrini, A. Marinelli, and S. Reiche, “The physics of x-ray free-electron lasers,” *Reviews of Modern Physics* **88**, 015006 (2016).
- ³²M. Chergui and A. H. Zewail, “Electron and x-ray methods of ultrafast structural dynamics: Advances and applications,” *ChemPhysChem* **10**, 28–43 (2009).
- ³³J. Yang, X. Zhu, J. P. F. Nunes, J. K. Yu, R. M. Parrish, T. J. Wolf, M. Centurion, M. Gühr, R. Li, Y. Liu, *et al.*, “Simultaneous observation of nuclear and electronic dynamics by ultrafast electron diffraction,” *Science* **368**, 885–889 (2020).
- ³⁴T. Katayama, T.-K. Choi, D. Khakhulin, A. O. Dohn, C. J. Milne, G. Vankó, Z. Németh, F. A. Lima, J. Szlachetko, T. Sato, *et al.*, “Atomic-scale observation of solvent reorganization influencing photoinduced structural dynamics in a copper complex photosensitizer,” *Chemical Science* **14**, 2572–2584 (2023).
- ³⁵M. Minitti, J. Budarz, A. Kirrander, J. Robinson, D. Ratner, T. Lane, D. Zhu, J. Glowacki, M. Kozina, H. Lemke, *et al.*, “Imaging molecular motion: Femtosecond x-ray scattering of an electrocyclic chemical reaction,” *Physical Review Letters* **114**, 255501 (2015).
- ³⁶“TURBOMOLE V7.4.0 2019, a development of University of Karlsruhe and Forschungszentrum Karlsruhe GmbH, 1989-2007, TURBOMOLE GmbH, since 2007; available from <http://www.turbomole.com>.”.
- ³⁷R. Ahlrichs, M. Bär, M. Häser, H. Horn, and C. Kölmel, “Electronic structure calculations on workstation computers: The program system turbomole,” *Chemical Physics Letters* **162**, 165–169 (1989).
- ³⁸C. Adamo and V. Barone, “Toward reliable density functional methods without adjustable parameters: The pbe0 model,” *The Journal of Chemical Physics* **110**, 6158–6170 (1999).
- ³⁹T. H. Dunning, “Gaussian basis sets for use in correlated molecular calculations. i. the atoms boron through neon and hydrogen,” *The Journal of Chemical Physics* **90**, 1007–1023 (1989).
- ⁴⁰R. A. Kendall, T. H. Dunning, and R. J. Harrison, “Electron affinities of the first-row atoms revisited. systematic basis sets and wave functions,” *The Journal of Chemical Physics* **96**, 6796–6806 (1992).
- ⁴¹S. Hirata and M. Head-Gordon, “Time-dependent density functional theory within the tamm-dancoff approximation,” *Chemical Physics Letters* **314**, 291–299 (1999).

- ⁴²C. D. Rankine, “Optci gitlab page,” .
- ⁴³F. Neese, “The orca program system,” *WIREs Computational Molecular Science* **2**, 73–78 (2011).
- ⁴⁴F. Neese, “Software update: the orca program system,” *WIREs Computational Molecular Science* **8**, e1327 (2017).
- ⁴⁵H. Köppel, W. Domcke, and L. S. Cederbaum, “The multi-mode vibronic coupling approach,” *Conical Intersections* , 323–367 (2004).
- ⁴⁶L. S. Cederbaum, H. Köppel, and W. Domcke, “Multimode vibronic coupling effects in molecules,” *International Journal of Quantum Chemistry* **20**, 251–267 (2009).
- ⁴⁷T. J. Penfold and G. A. Worth, “A model hamiltonian to simulate the complex photochemistry of benzene ii,” *The Journal of Chemical Physics* **131** (2009).
- ⁴⁸T. Penfold, R. Spesytysev, O. Kirkby, R. Minns, D. Parker, H. Fielding, and G. Worth, “Quantum dynamics study of the competing ultrafast intersystem crossing and internal conversion in the “channel 3” region of benzene,” *The Journal of Chemical Physics* **137** (2012).
- ⁴⁹T. J. Penfold and J. Eng, “Mind the gap: Quantifying the breakdown of the linear vibronic coupling hamiltonian,” *Physical Chemistry Chemical Physics* **25**, 7195–7204 (2023).
- ⁵⁰T. Pope, J. Eng, A. Monkman, and T. J. Penfold, “Spin-vibronic intersystem crossing and molecular packing effects in heavy-atom-free organic phosphor,” *Journal of Chemical Theory and Computation* (2024), 10.1021/acs.jctc.3c01220.
- ⁵¹Eng, J., “Vibronic coupling maker,” .
- ⁵²M. H. Beck, A. Jäckle, G. A. Worth, and H.-D. Meyer, “The multiconfigurational time-dependent hartree (mctdh) method: A highly efficient algorithm for propagating wavepackets,” *Physics Reports* **324**, 1–105 (2000).
- ⁵³H.-D. Meyer, F. Gatti, and G. A. Worth, *Multidimensional Quantum Dynamics: MCTDH Theory and Applications* (John Wiley & Sons, 2009).
- ⁵⁴G. Worth, K. Giri, G. Richings, I. Burghardt, M. Beck, A. Jäckle, and H. Meyer, “The quantics package, version 1.1, university of birmingham, birmingham, u.k.”.
- ⁵⁵M. Barbatti, M. Ruckebauer, F. Plasser, J. Pittner, G. Granucci, M. Persico, and H. Lischka, “Newton-x: A surface-hopping program for nonadiabatic molecular dynamics,” *WIREs Computational Molecular Science* **4**, 26–33 (2013).
- ⁵⁶M. Barbatti, G. Granucci, M. Persico, M. Ruckebauer, M. Vazdar, M. Eckert-Maksić, and H. Lischka, “The on-the-fly surface-hopping program system newton-x: Application to ab initio

- simulation of the nonadiabatic photodynamics of benchmark systems,” *Journal of Photochemistry and Photobiology A: Chemistry* **190**, 228–240 (2007).
- ⁵⁷L. Verlet, “Computer experiments on classical fluids. i. thermodynamical properties of lennard-jones molecules,” *Physical Review* **159**, 98–103 (1967).
- ⁵⁸W. C. Swope, H. C. Andersen, P. H. Berens, and K. R. Wilson, “A computer simulation method for the calculation of equilibrium constants for the formation of physical clusters of molecules: Application to small water clusters,” *The Journal of Chemical Physics* **76**, 637–649 (1982).
- ⁵⁹S. Hammes-Schiffer and J. C. Tully, “Proton transfer in solution: Molecular dynamics with quantum transitions,” *The Journal of Chemical Physics* **101**, 4657–4667 (1994).
- ⁶⁰M. T. do Casal, J. M. Toldo, M. Pinheiro Jr, and M. Barbatti, “Fewest-switches surface hopping with baec-an couplings,” *Open Research Europe* **1**, 49 (2021).
- ⁶¹E. Marsili, A. Prlj, and B. F. Curchod, “Caveat when using adc (2) for studying the photochemistry of carbonyl-containing molecules,” *Physical Chemistry Chemical Physics* **23**, 12945–12949 (2021).
- ⁶²E. K. Lee, R. G. Shortridge Jr, and C. F. Rusbult, “Fluorescence excitation study of cyclobutanone, cyclopentanone, and cyclohexanone in the gas phase,” *Journal of the American Chemical Society* **93**, 1863–1867 (1971).
- ⁶³T. Penfold and G. Worth, “The effect of molecular distortions on spin-orbit coupling in simple hydrocarbons,” *Chemical Physics* **375**, 58–66 (2010).
- ⁶⁴T. J. Penfold, E. Gindensperger, C. Daniel, and C. M. Marian, “The spin-vibronic mechanism for intersystem crossing,” *Chemical Reviews* **118**, 6975–7025 (2018).
- ⁶⁵A. M. S. Daría, J. Hernández-Rodríguez, L. M. Ibele, and S. Gómez, “Photofragmentation of cyclobutanone at 200 nm: Td-dft vs casscf electron diffraction,” (2024), arXiv:2401.07597 [physics.chem-ph].
- ⁶⁶J. Janoš, J. P. F. Nunes, D. Hollas, P. Slavíček, and B. F. E. Curchod, “Predicting the photodynamics of cyclobutanone triggered by a laser pulse at 200 nm and its mev-ued signals – a trajectory surface-hopping and xms-caspt2 perspective,” (2024), arXiv:2402.05801 [physics.chem-ph].
- ⁶⁷S. Thompson, J. Eng, and T. J. Penfold, “The intersystem crossing of a cyclic (alkyl)(amino) carbene gold (i) complex,” *The Journal of Chemical Physics* **149** (2018), 10.1063/1.5032185.
- ⁶⁸J. Eng, S. Thompson, H. Goodwin, D. Credgington, and T. J. Penfold, “Competition between the heavy atom effect and vibronic coupling in donor–bridge–acceptor organometallics,” *Physical*

- Chemistry Chemical Physics **22**, 4659–4667 (2020).
- ⁶⁹Q. Gu, F. Chotard, J. Eng, A.-P. M. Reponen, I. J. Vitorica-Yrezabal, A. W. Woodward, T. J. Penfold, D. Credgington, M. Bochmann, and A. S. Romanov, “Excited-state lifetime modulation by twisted and tilted molecular design in carbene-metal-amide photoemitters,” *Chemistry of Materials* **34**, 7526–7542 (2022).
- ⁷⁰M. Baba and I. Hanazaki, “The $s1$ (n, π^*) states of cyclopentanone and cyclobutanone in a supersonic nozzle beam,” *The Journal of Chemical Physics* **81**, 5426–5433 (1984).
- ⁷¹G. Capano, T. Penfold, M. Chergui, and I. Tavernelli, “Photophysics of a copper phenanthroline elucidated by trajectory and wavepacket-based quantum dynamics: A synergetic approach,” *Physical Chemistry Chemical Physics* **19**, 19590–19600 (2017).
- ⁷²X. Miao, K. Diemer, and R. Mitrić, “A casscf/mrci trajectory surface hopping simulation of the photochemical dynamics and the gas phase ultrafast electron diffraction patterns of cyclobutanone,” (2024), arXiv:2401.06673 [physics.chem-ph].
- ⁷³J. Suchan, F. Liang, A. S. Durden, and B. G. Levine, “Prediction challenge: First principles simulation of the ultrafast electron diffraction spectrum of cyclobutanone,” (2024), arXiv:2401.08069 [physics.chem-ph].
- ⁷⁴J. P. Figueira Nunes, L. M. Ibele, S. Pathak, A. R. Attar, S. Bhattacharyya, R. Boll, K. Borne, M. Centurion, B. Erk, M.-F. Lin, *et al.*, “Monitoring the evolution of relative product populations at early times during a photochemical reaction,” *arXiv e-prints*, arXiv–2311 (2023).

The Photochemistry of Rydberg Excited Cyclobutanone: Photoinduced Processes and Ground State Dynamics

Supplementary Information

J. Eng^a, C. D. Rankine^b, T. J. Penfold^a

^a Chemistry, School of Natural and Environmental Sciences, Newcastle University, Newcastle upon Tyne, NE1 7RU, UK

^b Department of Chemistry, University of York, York, YO10 5DD, UK

tom.penfold@newcastle.ac.uk

julien.eng@newcastle.ac.uk

Contents

S1 Electronic Structure of Cyclobutanone	4
S1-1 Method and Basis Set Dependence of Excited States at the Franck-Condon Geometry . . .	4
S1-2 ADC(2) and LR-TDDFT Excited State Energies at S ₁ and S ₂ Optimised Geometries . . .	5
S1-3 Molecular Orbitals of Cyclobutanone	7
S1-4 Potential Energy Curve along C=O Breathing Mode	8
S1-5 Linear Reaction Coordinates leading to Conical Intersections	9
S2 Quantum Dynamics	10
S2-1 Normal Modes	10
S2-2 Model Hamiltonian Expansion Coefficients	11
S2-3 Quantum Dynamics Simulations	13
S3 Trajectory Surface Hopping using ADC(2) Potentials	13
S4 Key Geometries	17

List of Tables

S1	Low lying singlet excited state of cyclobutanone calculated using ADC(2), LR-TDDFT(PBE0) and NEVPT2(6,6) as a function of basis set at the ground state optimised geometry. For the NEVPT2, due to the size of the active space used only the S ₁ and S ₂ are included in the calculations.	4
S2	Low lying singlet excited state of cyclobutanone calculated using NEVPT2 as a function of size of the active space calculated using the aug-cc-pVDZ basis set.	4
S3	Summary of electronic energies, characters, and symmetries of the ground- (GS) and electronically-excited (S _n /T _n ; n = [1..5]) states of cyclobutanone evaluated at the S ₁ minimum-energy geometry and at the ADC(2)/aug-cc-pVTZ and LR-TDDFT(PBE0)/aug-cc-pVDZ levels of theory. Comparative tables for evaluations at the S ₁ - (Table S3) and S ₂ -state (Table S4) minimum-energy geometries are presented in the SI. The relevant molecular orbitals are shown in the SI. The HOMO is designated as H; the LUMO is designated as L.	5

S4	Summary of electronic energies, characters, and symmetries of the ground- (GS) and electronically-excited (S_n/T_n ; $n = [1..5]$) states of cyclobutanone evaluated at the S_2 minimum-energy geometry and at the ADC(2)/aug-cc-pVTZ and LR-TDDFT(PBE0)/aug-cc-pVDZ levels of theory. Comparative tables for evaluations at the S_1 - (Table S3) and S_2 -state (Table S4) minimum-energy geometries are presented in the SI. The relevant molecular orbitals are shown in the SI. The HOMO is designated as H; the LUMO is designated as L.	6
S5	Expansion Coefficients used for the model Hamiltonian used within this work.	11
S6	Expansion Coefficients used for the model Hamiltonian used within this work.	12
S7	Spin-orbit coupling η in cm^{-1} between the electronic states included in the Hamiltonian. .	12
S8	Computational details for the MCTDH simulations of the model presented in this work. N_i, N_j are the number of primitive harmonic oscillator discrete variable representation (DVR) basis functions used to describe each mode. n_{SPF} is the number of single-particle functions used to describe the wavepacket on each state.	13
S9	Ground state geometry optimised using DFT(PBE0)/aug-cc-pvdz.	17
S10	Excited S_1 excited state geometry optimised using LR-TDDFT(PBE0)/aug-cc-pvdz. . . .	17
S11	Excited S_2 excited state geometry optimised using LR-TDDFT(PBE0)/aug-cc-pvdz. . . .	18
S12	S_2/S_1 conical intersection geometry optimised using LR-TDDFT(PBE0)/aug-cc-pvdz. . .	18
S13	S_1/S_0 C_α conical intersection geometry optimised using LR-TDDFT(PBE0)/aug-cc-pvdz. .	18
S14	S_1/S_0 C_β conical intersection geometry optimised using LR-TDDFT(PBE0)/aug-cc-pvdz. .	19
S15	S_1/S_0 C_α, C_β conical intersection geometry optimised using LR-TDDFT(PBE0)/aug-cc-pvdz. .	19

List of Figures

S1	Molecular orbitals of cyclobutanone involved in the lowest excited states reported here and in the main text.	7
S2	S_0/S_1 potential Energy Surface along ν_{21} , C=O stretching normal mode using NEVPT2(12,12)/aug-cc-pvtz (black dashed), LR-TDDFT(PBE0)/aug-cc-pvtz (green) and ADC(2)/aug-cc-pvtz (blue dashed) levels of theory. This clearly shows the artificial crossing for ADC(2) consistent with the observations of ref. [1].	8
S3	DFT/LR-TDDFT(PBE0)/aug-cc-pvdz potential energy surface along a linear reaction coordinate from the Franck-Condon to the conical intersection between the S_2/S_1 states. . .	9
S4	DFT/LR-TDDFT(PBE0)/aug-cc-pvdz potential energy surface along a linear reaction coordinate from (a) the S_1 minimum energy geometry to C_α conical intersection between the S_1/S_0 states, (b) the S_1 minimum energy geometry to C_β conical intersection between the S_1/S_0 states and (c) the S_1 minimum energy geometry to C_α, C_β conical intersection between the S_1/S_0 states. Structures are shown in the main text and the cartesian coordinates are provided below.	9
S5	Normal modes of cyclobutanone included in the model Hamiltonian used within this work. .	10
S6	Excited state population kinetics extracted from 69 <i>on-the-fly</i> trajectory surface hopping trajectories after vertical excitation into the S_2 (blue) following the decay into the S_1 (red) and ground (black) state. All trajectories included were propagation for 500fs.	13
S7	Average C_α and CO bond lengths for the structure of cyclobutanone where the trajectory hops from S_2-S_1 (a) and S_1-S_0 (b).	14
S8	Transient scattering ($\Delta I/I$) without (a) and with (b) 150 fs temporal broadening. Transient PDF without (c) and with (d) 150 fs temporal broadening. The ground state curves used to generate the transient were obtained from the initial conditions, <i>i.e.</i> at $t=0$. All these plots have been calculated using the 69 500 fs trajectories.	15

S9	Initial (t=0, black) and final (t=2000 fs, grey) PDF and their difference (red) calculated using the 289 2000 fs surface hopping trajectories simulated using potentials are ADC(2) level of theory.	16
----	--	----

S1 Electronic Structure of Cyclobutantone

S1-1 Method and Basis Set Dependence of Excited States at the Franck-Condon Geometry

ADC(2)						
State	cc-pVDZ	cc-pVTZ	cc-pVQZ	aug-cc-pVDZ	aug-cc-pVTZ	aug-cc-pVQZ
S ₁	4.30	4.26	4.26	4.20	4.21	4.23
S ₂	7.70	7.16	6.89	5.76	5.99	6.12
S ₃	8.38	8.02	7.66	6.34	6.53	6.68
S ₄	8.60	8.19	8.00	6.50	6.64	6.81
S ₅	8.63	8.37	8.19	6.51	6.68	6.84

TDDFT(PBE0)						
State	cc-pVDZ	cc-pVTZ	cc-pVQZ	aug-cc-pVDZ	aug-cc-pVTZ	aug-cc-pVQZ
S ₁	4.34	4.35	4.34	4.31	4.33	4.33
S ₂	7.54	7.06	6.78	6.08	6.10	6.09
S ₃	7.74	7.63	7.58	6.68	6.67	6.66
S ₄	7.86	7.78	7.62	6.79	6.77	6.75
S ₅	8.20	8.00	7.73	6.80	6.78	6.76

NEVPT2(6,6)						
State	cc-pVDZ	cc-pVTZ	cc-pVQZ	aug-cc-pVDZ	aug-cc-pVTZ	aug-cc-pVQZ
S ₁	4.47	4.50	4.52	4.55	4.55	–
S ₂	8.14	7.62	7.38	6.47	6.72	–

Table S1: Low lying singlet excited state of cyclobutantone calculated using ADC(2), LR-TDDFT(PBE0) and NEVPT2(6,6) as a function of basis set at the ground state optimised geometry. For the NEVPT2, due to the size of the active space used only the S₁ and S₂ are included in the calculations.

State	NEVPT2(2,2)	NEVPT2(4,4)	NEVPT2(6,6)	NEVPT2(8,8)	NEVPT2(12,12)
S ₁	4.42	4.36	4.55	4.65	4.48
S ₂	10.68	8.57	6.47	6.51	6.43

Table S2: Low lying singlet excited state of cyclobutantone calculated using NEVPT2 as a function of size of the active space calculated using the aug-cc-pVDZ basis set.

^{0†} Electronic Supplementary Information (ESI) available: [details of any supplementary information available should be included here]. See DOI: 10.1039/cXCP00000x/

S1-2 ADC(2) and LR-TDDFT Excited State Energies at S_1 and S_2 Optimised Geometries

State	ADC(2)		LR-TDDFT(PBE0)	
	Energy / eV	Character (Irrep.)	Energy / eV	Character (Irrep.)
GS	1.13	— (A')	0.93	— (A')
S_1	3.96	H \rightarrow L (A'')	4.02	H \rightarrow L (A'')
S_2	6.96	H \rightarrow L+1 (A'')	7.03	H \rightarrow L+1 (A'')
S_3	7.36	H-2 \rightarrow L (A'')	7.17	H-2 \rightarrow L (A'')
S_4	7.49	H-1 \rightarrow L (A')	7.30	H-1 \rightarrow L (A')
		H-4 \rightarrow L		H-4 \rightarrow L
T_1	3.56	H \rightarrow L (A'')	3.38	H \rightarrow L (A'')
T_2	5.99	H-1 \rightarrow L (A')	5.71	H-1 \rightarrow L (A')
		H-4 \rightarrow L		H-4 \rightarrow L
T_3	6.93	H-2 \rightarrow L (A'')	6.78	H-2 \rightarrow L (A'')
T_4	7.30	H-3 \rightarrow L (A')	7.19	H-3 \rightarrow L (A')

Table S3: Summary of electronic energies, characters, and symmetries of the ground- (GS) and electronically-excited (S_n/T_n ; $n = [1..5]$) states of cyclobutanone evaluated at the S_1 minimum-energy geometry and at the ADC(2)/aug-cc-pVTZ and LR-TDDFT(PBE0)/aug-cc-pVDZ levels of theory. Comparative tables for evaluations at the S_1 - (Table S3) and S_2 -state (Table S4) minimum-energy geometries are presented in the SI. The relevant molecular orbitals are shown in the SI. The HOMO is designated as H; the LUMO is designated as L.

State	ADC(2)		LR-TDDFT(PBE0)	
	Energy / eV	Character (Irrep.)	Energy / eV	Character (Irrep.)
GS	0.51	— (A')	0.51	— (A')
S ₁	4.79	H→L (A ₂ [A''])	4.72	H→L (A'')
S ₂	5.86	H→L+1 (B ₁ [A'])	5.84	H→L+1 (A')
S ₃	6.52	H→L+4 (A ₂ [A''])	6.54	H→L+3 (A'')
S ₄	6.58	H→L+2 (B ₁ [A'])	6.56	H→L+2 (A')
T ₁	4.44	H→L (A ₁ [A'])	4.13	H→L (A'')
T ₂	5.79	H-1→L (A ₂ [A''])	5.73	H-1→L (A')
		H-4→L		H-4→L
T ₃	6.50	H→L+1 (A ₂ [A''])	6.44	H→L+1 (A'')
T ₄	6.54	H→L+3 (A ₁ [A'])	6.59	H→L+3 (A')

Table S4: ummary of electronic energies, characters, and symmetries of the ground- (GS) and electronically-excited (S_n/T_n; $n = [1..5]$) states of cyclobutanone evaluated at the S₂ minimum-energy geometry and at the ADC(2)/aug-cc-pVTZ and LR-TDDFT(PBE0)/aug-cc-pVDZ levels of theory. Comparative tables for evaluations at the S₁- (Table S3) and S₂-state (Table S4) minimum-energy geometries are presented in the SI. The relevant molecular orbitals are shown in the SI. The HOMO is designated as H; the LUMO is designated as L.

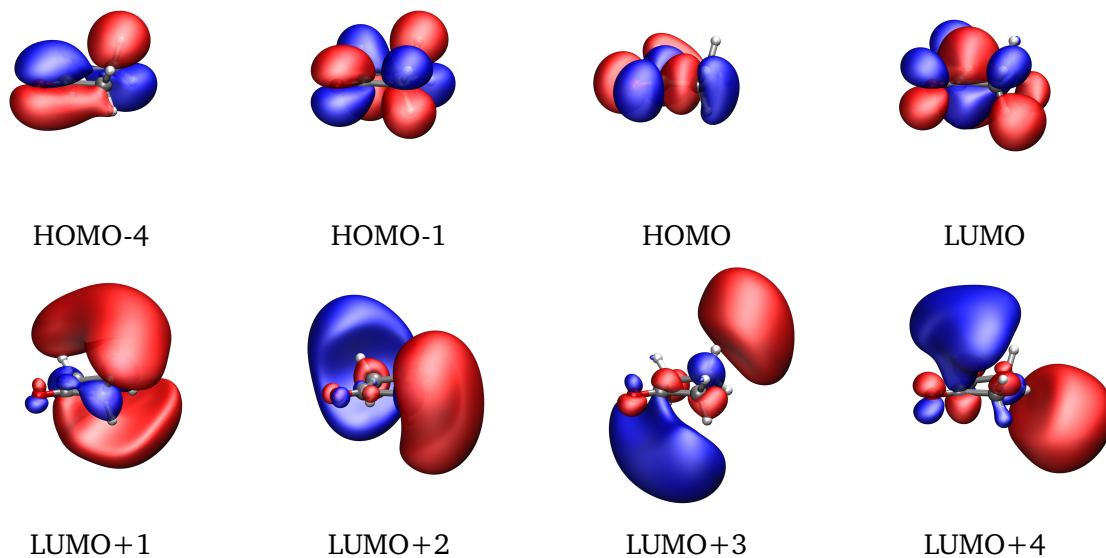
S1-3 Molecular Orbitals of Cyclobutanone

Figure S1: Molecular orbitals of cyclobutanone involved in the lowest excited states reported here and in the main text.

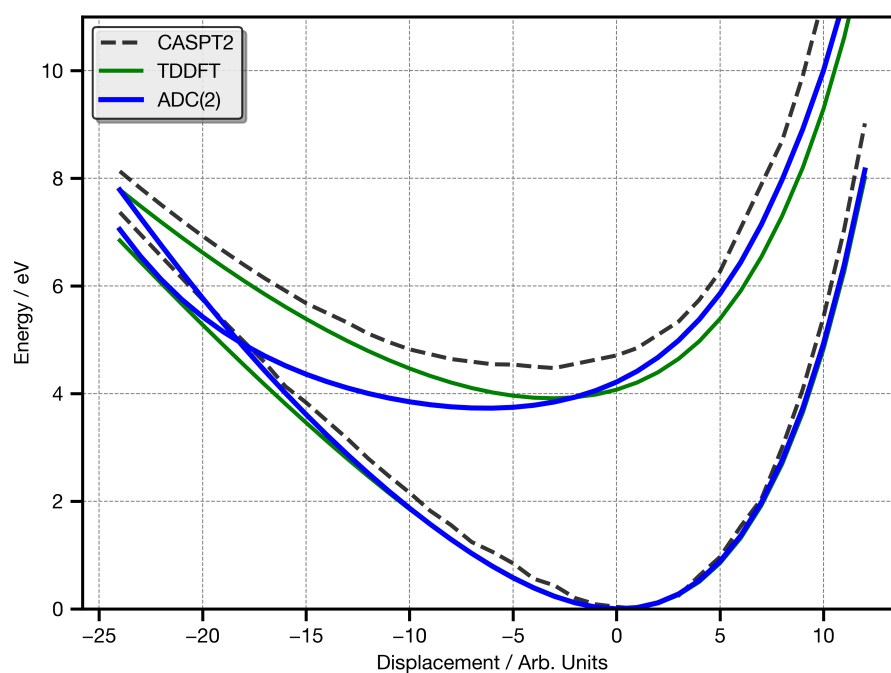
S1-4 Potential Energy Curve along C=O Breathing Mode

Figure S2: S_0/S_1 potential Energy Surface along ν_{21} , C=O stretching normal mode using NEVPT2(12,12)/aug-cc-pvtz (black dashed), LR-TDDFT(PBE0)/aug-cc-pvtz (green) and ADC(2)/aug-cc-pvtz (blue dashed) levels of theory. This clearly shows the artificial crossing for ADC(2) consistent with the observations of ref. [1].

S1-5 Linear Reaction Coordinates leading to Conical Intersections

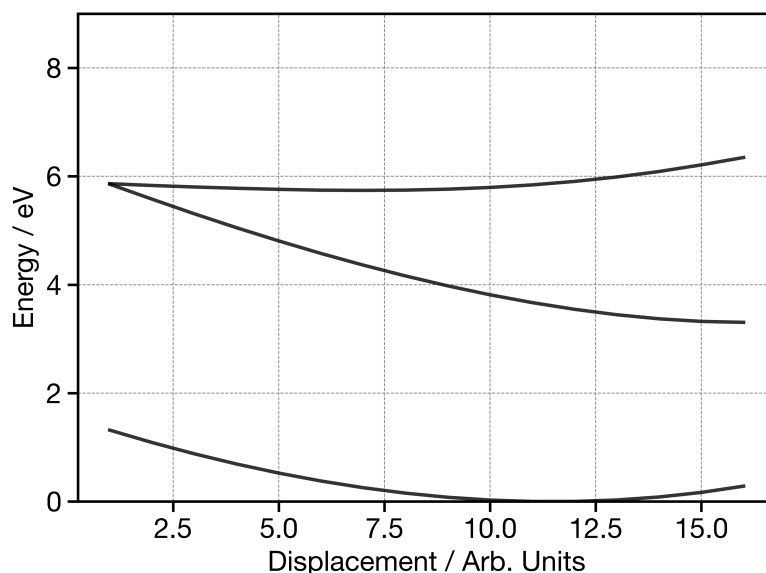


Figure S3: DFT/LR-TDDFT(PBE0)/aug-cc-pvdz potential energy surface along a linear reaction coordinate from the Franck-Condon to the conical intersection between the S_2/S_1 states.

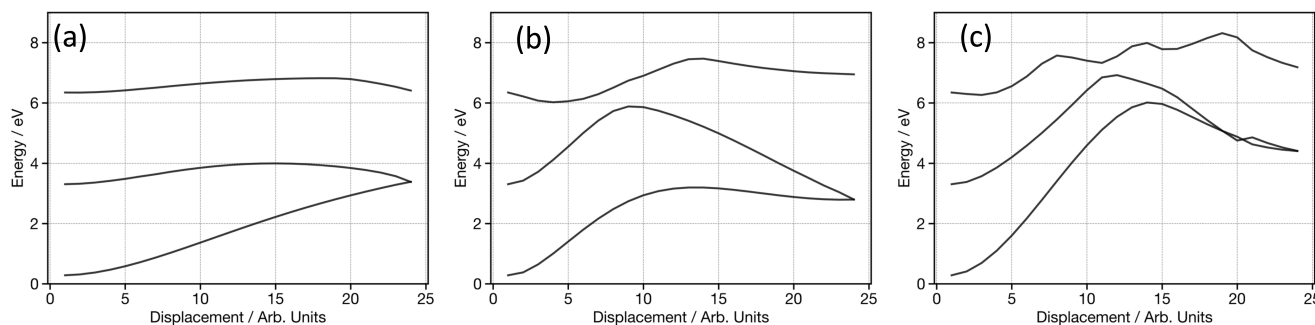


Figure S4: DFT/LR-TDDFT(PBE0)/aug-cc-pvdz potential energy surface along a linear reaction coordinate from (a) the S_1 minimum energy geometry to C_α conical intersection between the S_1/S_0 states, (b) the S_1 minimum energy geometry to C_β conical intersection between the S_1/S_0 states and (c) the S_1 minimum energy geometry to C_α , C_β conical intersection between the S_1/S_0 states. Structures are shown in the main text and the cartesian coordinates are provided below.

S2 Quantum Dynamics

S2-1 Normal Modes

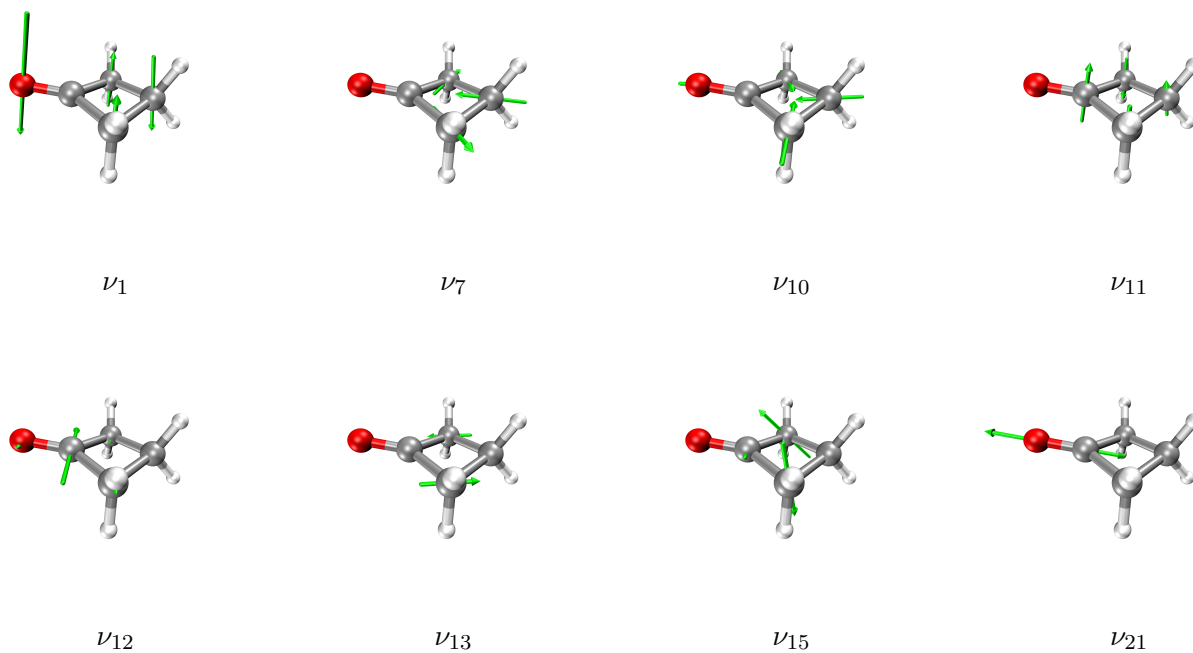


Figure S5: Normal modes of cyclobutanone included in the model Hamiltonian used within this work.

S2-2 Model Hamiltonian Expansion Coefficients

Mode (a')	κ / eV									
	Singlets					Triplets				
	GS	S_1	S_2	S_3	S_4	T_1	T_2	T_3	t_4	T_5
Q_1	0.000	0.052	0.024	0.011	0.024	0.055	0.016	0.055	-0.017	0.023
Q_7	0.000	-0.001	0.022	0.016	0.010	0.018	0.036	0.029	0.031	-0.003
Q_{12}	0.000	0.050	-0.028	-0.017	-0.001	0.020	0.030	0.030	0.030	0.040
Q_{15}	0.000	-0.006	-0.128	-0.136	-0.116	0.002	-0.128	0.049	-0.131	-0.114
Mode (a')	γ / eV									
	Singlets					Triplets				
	GS	S_1	S_2	S_3	S_4	T_1	T_2	T_3	t_4	T_5
Q_1	0.010	0.001	0.007	0.005	0.007	0.005	0.009	-0.011	0.005	0.004
Q_7	-0.026	-0.027	-0.028	-0.029	-0.029	-0.027	-0.027	-0.028	-0.029	-0.030
Q_{12}	0.001	-0.022	-0.009	-0.009	-0.009	-0.020	-0.020	-0.020	-0.020	0.020
Q_{15}	0.069	-0.074	-0.073	-0.073	-0.070	-0.073	-0.077	-0.092	-0.078	-0.074
Mode (a')	δ / eV									
	Singlets					Triplets				
	GS	S_1	S_2	S_3	S_4	T_1	T_2	T_3	t_4	T_5
Q_1	0.002	0.002	0.002	0.002	0.002	0.002	0.002	0.003	0.002	0.003
Q_7	—	—	—	—	—	—	—	—	—	—
Q_{12}	—	—	—	—	—	—	—	—	—	—
Q_{15}	—	—	—	—	—	—	—	—	—	—

Table S5: Expansion Coefficients used for the model Hamiltonian used within this work.

Q_{10}	Singlets					Triplets				
	GS	S_1	S_2	S_3	S_4	T_1	T_2	T_3	t_4	T_5
D	11.714	2.642	2.547	2.627	2.382	5.167	2.464	13.518	3.432	2.000
α	0.101	0.117	0.163	0.161	0.161	0.102	0.167	0.066	0.143	0.174
x_e	0.00	3.008	0.158	0.205	0.254	2.363	0.006	4.126	0.158	0.110
$\delta\varepsilon$	0.000	-0.484	-0.035	-0.026	-0.020	-0.441	-0.027	1.351	-0.059	-0.002
Q_{21}	Singlets					Triplets				
	GS	S_1	S_2	S_3	S_4	T_1	T_2	T_3	t_4	T_5
D	20.890	17.810	18.950	9.640	15.970	17.910	18.880	18.100	7.070	14.090
α	0.055	0.057	0.056	0.072	0.060	0.057	0.056	0.056	0.080	0.063
x_e	0.000	-0.064	-0.189	-0.011	-0.084	-0.122	-0.186	0.084	0.080	-0.053
$\delta\varepsilon$	0.000	0.008	-0.009	-0.017	-0.017	0.003	0.005	0.002	-0.006	0.001

Table S6: Expansion Coefficients used for the model Hamiltonian used within this work.

η / cm^{-1}	T_1	T_2	T_3	T_4	S_1	S_2	S_3	S_4
T_1	—	54.49	0.32	2.19	0.02	0.43	0.94	0.00
T_2	54.49	—	0.74	3.30	0.00	0.00	0.00	-0.20
T_3	0.32	0.74	—	0.05	0.14	0.01	-0.04	0.00
T_4	2.19	3.30	0.05	—	-1.48	0.03	0.01	0.00

Table S7: Spin-orbit coupling η in cm^{-1} between the electronic states included in the Hamiltonian.

S2-3 Quantum Dynamics Simulations

Modes	N_i	N_j	n_{SPF}									
			GS	S_1	S_2	S_3	S_4	T_1	T_2	T_3	T_4	T_5
$\nu_1 \quad \nu_7$	41	41	1	18	12	12	12	2	2	2	2	2
$\nu_{11} \quad \nu_{13}$	41	41	1	18	12	12	12	2	2	2	2	2
$\nu_{10} \quad \nu_{12}$	41	41	1	18	12	12	12	2	2	2	2	2
$\nu_{15} \quad \nu_{21}$	41	89	1	18	12	12	12	2	2	2	2	2

Table S8: Computational details for the MCTDH simulations of the model presented in this work. N_i, N_j are the number of primitive harmonic oscillator discrete variable representation (DVR) basis functions used to describe each mode. n_{SPF} is the number of single-particle functions used to describe the wavepacket on each state.

S3 Trajectory Surface Hopping using ADC(2) Potentials

ADC(2) often represents an excellent approach to perform excited state dynamics owing to its favourable balance between computational efficiency and accuracy as well as its increased stability compared to methods such as CC2 [2]. However, as discussed in ref. [1] and shown above in Figure S2, it shows artificial crossing between the ground and first excited state along the C=O stretch. To understand the influence this has on the excited state dynamics and the ultrafast electron diffraction, we have performed excited state dynamics using ADC(2) potentials, and the results are now discussed.

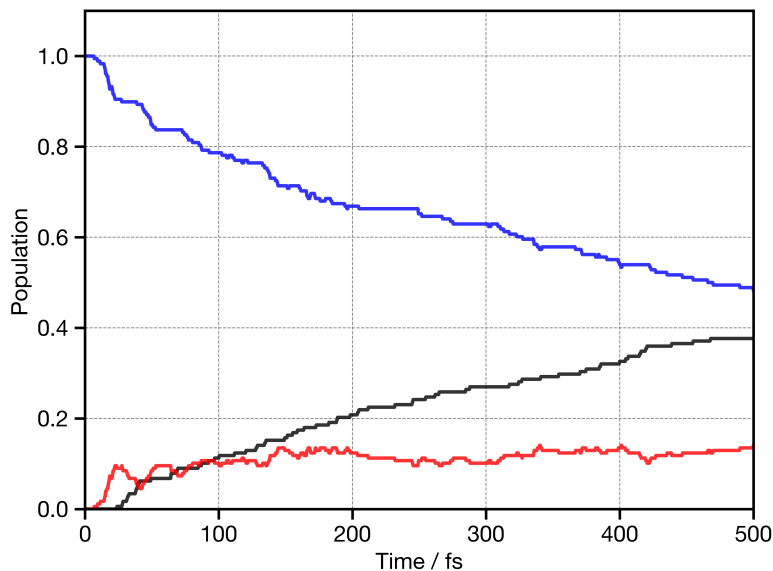


Figure S6: Excited state population kinetics extracted from 69 *on-the-fly* trajectory surface hopping trajectories after vertical excitation into the S_2 (blue) following the decay into the S_1 (red) and ground (black) state. All trajectories included were propagated for 500fs.

Figure S6 shows the relative populations of the S_2 , S_1 and ground state for the first 500 fs after excitation into the $S_2(n \rightarrow 3s)$ state obtained from 69 trajectories, ran for 500 fs. This shows a comparable, but slightly slower decay of the S_2 state than observed for LR-TDDFT(PBE0) and the quantum dynamics

shown in the main text. Indeed, this decay kinetics is actually in very close agreement with the photoelectron spectroscopic study performed in ref. [3]. In agreement with the LR-TDDFT(PBE0), once in the $S_1(n \rightarrow \pi^*)$ (red) state, the trajectories relax quickly into the electronic ground state (black) with a constant amount of $\sim 15\%$ remaining in the S_1 state.

Figure S7 shows an analysis of the hopping point of all the trajectories. This shows, consistent with the LR-TDDFT(PBE0) and model Hamiltonian dynamics presented in the main text that conversion from the $S_2 \rightarrow S_1$ occurs close to the Franck-Condon geometry. This fact that the dynamics is slow, despite the small structural displacements required to reach the crossing geometries reflects the weak nature of the coupling, which to first order is symmetry forbidden. In contrast, the hopping geometries of the conversion from the $S_1 \rightarrow S_0$ state demonstrates a larger displacement, primarily when the C=O distance is 1.6 \AA . As discussed above, is the point for the artificial crossing between the S_1 and S_0 state, which arises along the C=O stretch for ADC(2), but not LR-TDDFT(PBE0) or NEVPT2. The importance of this false crossing is clearly likely to bias the excited state dynamics simulations meaning that crossing to the ground state will more likely occur close to the Franck-Condon geometry with a elongated C=O bond rather than the ring open conformers identified in during previous work [4]. Indeed, this bias can be seen in the formation of the photoproducts, with only 7% of the trajectories exhibiting dissociative behaviour.

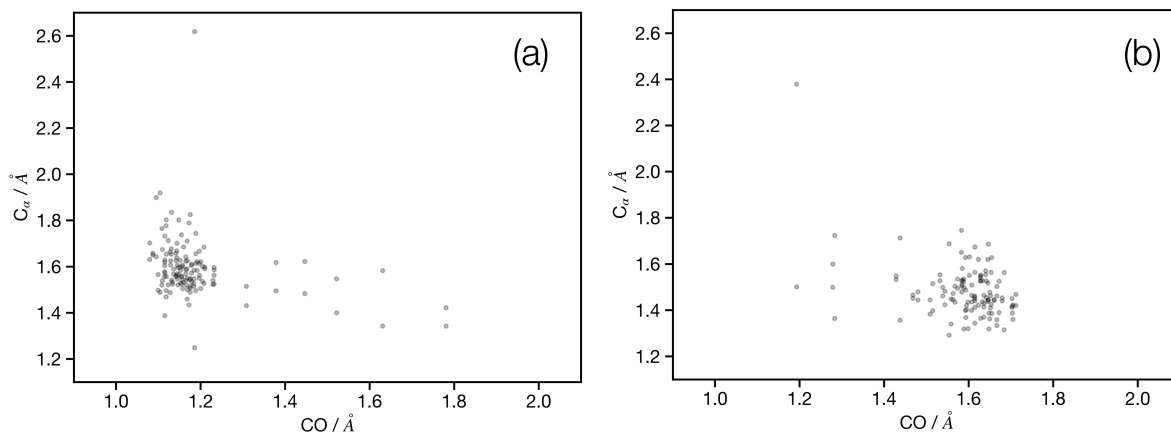


Figure S7: Average C_α and CO bond lengths for the structure of cyclobutanone where the trajectory hops from $S_2 \rightarrow S_1$ (a) and $S_1 \rightarrow S_0$ (b).

Figure S8 shows the time resolved electron diffraction simulations arising after photoexcitation of cyclobutanone into the S_2 state. Figure S8a shows the raw scattering signal, while Figure fig:trelectrondiffractionb has been broadened with a Gaussian with width of 150 fs, consistent with the temporal resolution of the experiment. Figures S8c and d show the sine transformation in the time-resolved PDF without and with temporal broadening, respectively. The time-resolved scattering curves exhibit broadly similar behaviour to the LR-TDDFT(PBE0) shown in the main text with strong 2 strong negative (~ 1 and 9 \AA^{-1}) and 2 positive (~ 2.7 and 7.5 \AA^{-1}) features. Importantly, each of the transient features exhibits a slight movement to small distances with time, suggesting an elongation of the average bond distances consistent with those trajectories that dissociate, but also the C=O bond changes discussed above.

The time-resolved PDFs (Figures S8c and d and Figure S9) also shows 2 negative peaks at 1.5 and 2.5 \AA , consistent with the LR-TDDFT(PBE0) dynamics. However, the relative ratio between these peaks is rather different, with the negative transition at 1.5 \AA being significantly stronger than the one at 2.5 \AA . This arises because although the fragmentation leads to the loss of both features, in the present dynamics, the much stronger changes in the C=O bond length moves intensity from the first. to the second peak, making the change in the first peak larger.

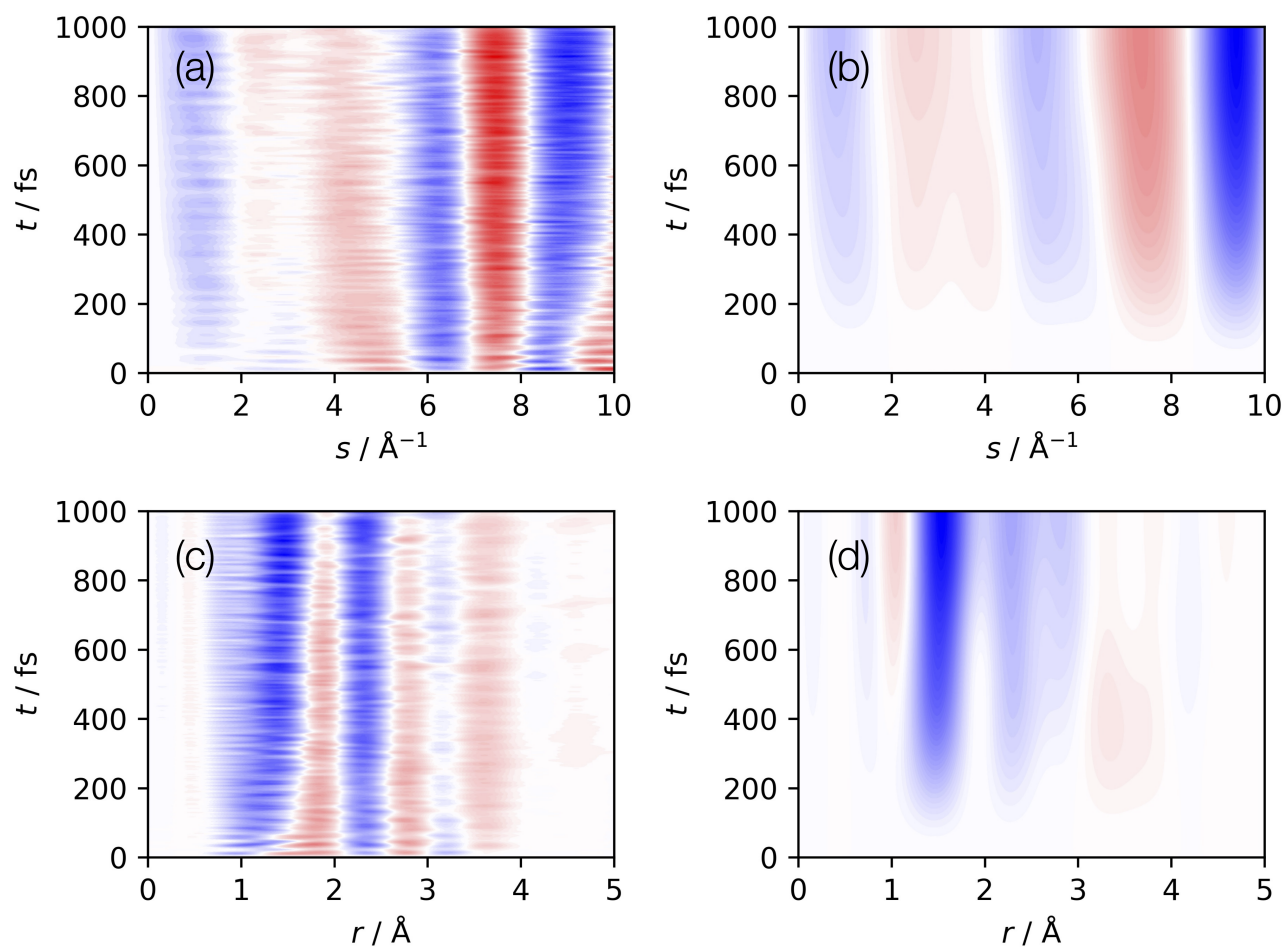


Figure S8: Transient scattering ($\Delta I/I$) without (a) and with (b) 150 fs temporal broadening. Transient PDF without (c) and with (d) 150 fs temporal broadening. The ground state curves used to generate the transient were obtained from the initial conditions, *i.e.* at $t=0$. All these plots have been calculated using the 69 500 fs trajectories.

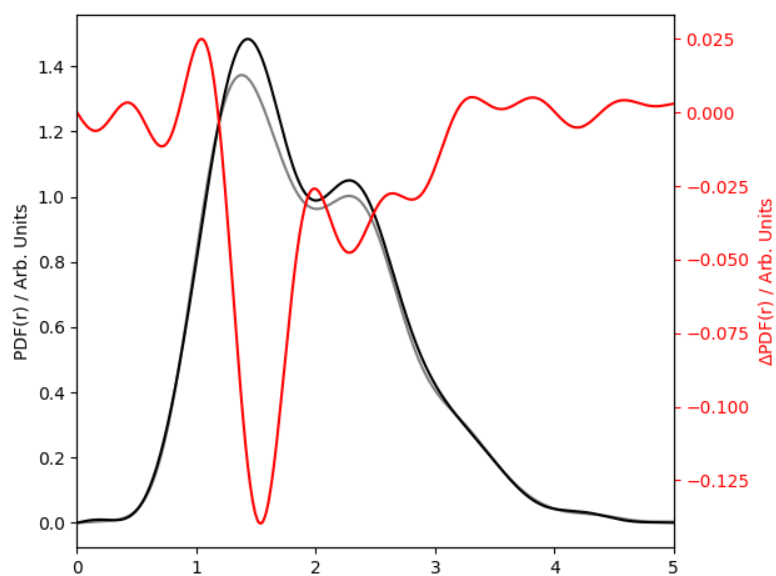


Figure S9: Initial ($t=0$, black) and final ($t=2000$ fs, grey) PDF and their difference (red) calculated using the 289 2000 fs surface hopping trajectories simulated using potentials are ADC(2) level of theory.

S4 Key Geometries

Atom	x (Å)	y (Å)	z (Å)
C	-0.22	0.64	0.00
C	-0.11	-0.41	-1.10
C	0.24	-1.45	0.00
C	-0.11	-0.41	1.10
O	-0.28	1.84	0.00
H	0.63	-0.21	-1.88
H	-1.08	-0.59	-1.58
H	-0.35	-2.36	0.00
H	1.31	-1.71	0.00
H	0.63	-0.21	1.88
H	-1.08	-0.59	1.58

Table S9: Ground state geometry optimised using DFT(PBE0)/aug-cc-pvdz.

Atom	x (Å)	y (Å)	z (Å)
C	0.04	0.70	0.00
C	-0.06	-0.42	-1.08
C	0.25	-1.47	0.00
C	-0.06	-0.42	1.08
O	-0.59	1.80	0.00
H	0.64	-0.28	-1.91
H	-1.10	-0.48	-1.46
H	-0.39	-2.35	0.00
H	1.30	-1.77	0.00
H	0.64	-0.28	1.91
H	-1.10	-0.48	1.46

Table S10: Excited S_1 excited state geometry optimised using LR-TDDFT(PBE0)/aug-cc-pvdz.

Atom	x (Å)	y (Å)	z (Å)
C	1.61	0.00	0.00
C	0.52	1.06	0.00
C	0.52	-1.06	0.00
C	-0.64	0.00	0.00
O	-1.80	0.00	-0.01
H	2.22	0.00	0.91
H	2.22	0.00	-0.90
H	0.39	1.62	0.94
H	0.40	1.63	-0.94
H	0.40	-1.63	-0.94
H	0.39	-1.63	0.94

Table S11: Excited S_2 excited state geometry optimised using LR-TDDFT(PBE0)/aug-cc-pvdz.

Atom	x (Å)	y (Å)	z (Å)
C	-0.31	0.64	-0.09
C	0.16	-0.43	-1.04
C	0.27	-1.53	-0.01
C	-0.12	-0.48	1.02
O	-0.51	1.80	-0.06
H	0.89	-0.12	-1.80
H	-1.18	-0.41	-1.16
H	-0.52	-2.30	-0.13
H	1.26	-1.96	0.13
H	0.73	-0.07	1.59
H	-1.09	-0.58	1.54

Table S12: S_2/S_1 conical intersection geometry optimised using LR-TDDFT(PBE0)/aug-cc-pvdz.

Atom	x (Å)	y (Å)	z (Å)
C	-0.13	0.87	0.26
C	-0.23	-0.82	-1.38
C	0.26	-1.47	-0.13
C	-0.07	-0.44	0.95
O	-0.61	1.92	0.12
H	0.29	0.11	-1.67
H	-0.62	-1.41	-2.21
H	-0.28	-2.40	0.08
H	1.34	-1.72	-0.10
H	0.65	-0.34	1.79
H	-1.07	-0.65	1.37

Table S13: S_1/S_0 C_α conical intersection geometry optimised using LR-TDDFT(PBE0)/aug-cc-pvdz.

Atom	x (Å)	y (Å)	z (Å)
C	0.07	0.55	0.04
C	0.66	-0.42	-1.17
C	2.04	-0.23	-1.48
C	-0.17	-0.11	1.25
O	-0.10	1.72	-0.25
H	0.00	-0.12	-1.99
H	0.43	-1.44	-0.81
H	2.82	-0.78	-0.94
H	2.36	0.50	-2.23
H	0.01	-1.18	1.36
H	-0.40	0.49	2.12

Table S14: S_1/S_0 C_β conical intersection geometry optimised using LR-TDDFT(PBE0)/aug-cc-pvdz.

Atom	x (Å)	y (Å)	z (Å)
C	-0.46	0.72	-0.26
C	0.78	-1.60	-1.92
C	0.40	-2.69	-1.23
C	0.43	-0.31	0.36
O	-1.66	0.49	-0.26
H	1.83	-1.33	-2.02
H	0.05	-1.03	-2.50
H	-0.65	-2.97	-1.14
H	1.13	-3.27	-0.64
H	1.44	0.02	0.61
H	0.13	-1.32	0.62

Table S15: S_1/S_0 C_α , C_β conical intersection geometry optimised using LR-TDDFT(PBE0)/aug-cc-pvdz.

References

- [1] Emanuele Marsili, Antonio Prlj, and Basile FE Curchod. Caveat when using adc (2) for studying the photochemistry of carbonyl-containing molecules. *Physical Chemistry Chemical Physics*, 23(23):12945–12949, 2021.
- [2] Felix Plasser, Rachel Crespo-Otero, Marek Pederzoli, Jiri Pittner, Hans Lischka, and Mario Barbatti. Surface hopping dynamics with correlated single-reference methods: 9h-adenine as a case study. *Journal of Chemical Theory and Computation*, 10(4):1395–1405, 2014.
- [3] Thomas S Kuhlman, Theis I Sølling, and Klaus B Møller. Coherent motion reveals non-ergodic nature of internal conversion between excited states. *ChemPhysChem*, 13(3):820–827, 2012.
- [4] Lihong Liu and Wei-Hai Fang. New insights into the photodissociation dynamics of cyclobutanone from aims dynamic simulation. *The Journal of Chemical Physics*, 144(14), 2016.